

Upscaling Of Cellulose Board Production Made From Hemp

by

**Bruno Manuel
Serrador Gonçalves**

Matriculation Nr.
9025163

Thesis
submitted to

University of Applied Sciences
Bonn-Rhein-Sieg

Department of
Natural Sciences

For the degree of

Master of Science

in

Material Sciences & Sustainability Methods

First examiner:

Prof. Dr. Bernhard Möginger

Second examiner:

Dr. Kathirvel Ganesan

Statutory declaration

I herewith declare that I have composed the present thesis myself and without use of any other than the cited sources and aids. Sentences or parts of sentences quoted literally are marked as such; other references regarding the statement and scope are indicated by full details of the publications concerned.

The thesis in the same or similar form has not been submitted to any examination body and has not been published. This thesis was not yet, even in part, used in another examination or as a course performance.

Place, Date

Signature

Abstract

The aim of this work is to develop a recipe for aerogel sheets made of hemp cellulose, suitable for an upscaling process with a specific device called CaProLi (**C**ellulose **A**erogel **P**roduction **L**ine). The goal is to use the aerogel sheets in the future as sustainable insulation boards made of hemp cellulose. The hemp cellulose was self-extracted from hemp fibers.

Two cellulose solutions, made of different commercial celluloses, were used as references using the CaProLi device in comparison to the ones developed within this work based on hemp cellulose. In addition, they were utilized to investigate a useful viscosity range for the upscaling process. Furthermore, one reference cellulose was used to investigate the gel point reduction on cellulose solutions with the addition of two different sodium salts. Additionally, the properties of the aerogels made of the different celluloses were investigated and compared. Furthermore, the influence of the sodium salt addition on the aerogel properties, as well as the influence of geometry and gelation solution, was investigated. The aerogel samples were characterized by determination of density (skeletal and envelope), porosity, volume shrinkage, BET surface area (N₂, gas sorption) and morphology (scanning electron microscopy, SEM). On top of this, Fourier transform infrared spectroscopy (FTIR) was done to approve the purity of the extracted hemp cellulose.

Looking at the results, the hemp cellulose aerogels showed the lowest envelope density and therefore the highest porosity of all cellulose aerogels. The nitrogen adsorption desorption analyses showed BET surface area values in the range of 190-320 m²/g, while there being differences between the geometries and therefore the gelation medium. Different pore distributions could be observed while comparing the sheet and monolithic samples, indicating a change in the porous network. There was no significant change in the usage of salts effecting the envelope density of the aerogel samples, as well as the porosity. The BET surface area and the pore size distribution was influenced by the addition of salts. Effects on the reduction of the gel point in the cellulose solution, were also observed with the addition of sodium salts. Additionally, the extracted hemp cellulose showed a good quality.

List of contents

1. INTRODUCTION.....	1
2. LITERATURE REVIEW.....	2
2.1. Biomass.....	2
2.2. Hemp.....	4
2.3. Cellulose.....	5
2.3.1. Overview	5
2.3.2. Morphology	6
2.3.3. Crystalline modifications.....	8
2.4. Aerogels	9
2.5. Cellulose aerogels	10
2.5.1. Overview	10
2.5.2. Dissolution mechanisms.....	10
2.5.3. Gelation mechanisms.....	13
3. EXPERIMENTAL PART.....	14
3.1. Materials	14
3.2. Methods.....	14
3.2.1. Rotational rheometry	14
3.2.2. Gas pycnometry	15
3.2.3. Quasi-fluid pycnometry.....	16
3.2.4. Gas sorption method.....	17
3.2.5. Scanning electron microscopy (SEM)	20
3.2.6. Fourier transform infrared spectroscopy (FTIR)	21
3.3. Extraction of cellulose and synthesis of aerogels.....	22
3.3.1. Grinding of hemp fibers	22
3.3.2. Cellulose extraction.....	22
3.3.3. Solution preparation	24
3.3.4. Monolith preparation.....	24
3.3.5. Sheet preparation.....	26
3.4. Measurements.....	28
3.4.1. Viscosity	28
3.4.2. Gel point.....	28
3.4.3. Densities and porosity	29
3.4.4. Volume shrinkage	30
3.4.5. Surface and pore size distribution	31
3.4.6. Morphology	32

3.4.7. FTIR	32
4. RESULTS AND DISCUSSION.....	33
4.1. Viscosity	33
4.1.1. C6288 cellulose.....	33
4.1.2. Sigmacell cellulose.....	33
4.1.3. Hemp cellulose.....	36
4.1.4. Comparison.....	36
4.2. Gel point	38
4.2.1. Cellulose solutions without salts.....	38
4.2.2. Cellulose solutions with salts.....	40
4.2.3. Solutions for CaProLi experiment.....	40
4.3. Densities.....	43
4.3.1. Skeletal density	43
4.3.2. Envelope density	44
4.4. Porosity	45
4.5. Volume shrinkage.....	46
4.6. Gas sorption.....	48
4.6.1. Adsorption isotherm and BET surface.....	48
4.6.2. Pore distribution	51
4.7. Morphology	56
4.8. FTIR.....	58
5. CONCLUSIONS.....	62
APPENDIX	63
LITERATURE	69

List of figures

Figure 1: Examples for the different groups of biomasses: a) woody biomass, b) herbaceous biomass, c) fruit biomass, d) aquatic biomass, e) contaminated biomass, f) animal and human waste [8-13]	2
Figure 2: Usage categories of biomass [6].....	3
Figure 3: Hemp (left) and cultivating countries of hemp (right) [21, 22].	4
Figure 4: Important cellulose sources: a) hard wood (beech tree), b) bamboo, c) cotton, d) sisal, e) tunicine, and f) Gluconacetobacter xylinum [24].	5
Figure 5: Structure of cellulose [26].	6
Figure 6: Morphology of cellulose: a) crystalline and amorphous structure in a microfibril, b) elementary building blocks [29, 30].	6
Figure 7: Hydrogen bonds in cellulose I (left) and cellulose II (right) [28].	7
Figure 8: Crystal modification of cellulose: a) cellulose I, b) cellulose II [24].....	8
Figure 9: Aerogel Classification [38].	9
Figure 10: Dissolution Mechanism with NMMO [40].	11
Figure 11: Dissolution mechanism with IL on the example of 1-butyl-3-methylimidazolium cation (C ₄ mim) and chloride [40].	11
Figure 12: Dissolution mechanism with organic solvents in combination with inorganic salts on the example of N,N-Dimethylacetamide (DMAc) with lithium chloride (LiCl) [40].	12
Figure 13: Process of cellulose dissolution with NaOH and Urea: a) cellulose bundle b) swollen cellulose c) dissolved cellulose [43].....	12
Figure 14: Common gelation mechanisms for polysaccharides: a) thermal treatment, b) ion-induced crosslinking, c) covalent crosslinking, d) pH-induced, e) anti-solvent [39].	13
Figure 15: Commonly used geometries: a) parallel plate, b) cone and plate, c) concentric cylinder [50].	14
Figure 16: Setup gas pycnometer [52].	15
Figure 17: Setup quasi-fluid pycnometer [55].	16
Figure 18: Different adsorption desorption isotherms [35].	17
Figure 19: SEM functionality (left) and penetration depth of different picture generating sources (right.) [35].....	20
Figure 20: FTIR setup [61].	21
Figure 21: Hemp fibers (left) and grinded hemp fibers (right).	22
Figure 22: Dried alkalization product (left) and dried cellulose after bleaching (right)	23
Figure 23: Cellulose aerogel monolith.	25
Figure 24: Setup CaProLi for sheet production.....	27
Figure 25: Cellulose aerogel sheet.	27
Figure 26: Cellulose solution viscosities with different weight concentration of C6288.	34
Figure 27: Comparison of Sigmacell and C6288 cellulose viscosity (7 wt%).	35
Figure 28: Viscosity of cellulose solutions with different concentrations of hemp cellulose.....	37
Figure 29: Example of gel point determination with C6288 cellulose solution.....	39
Figure 30: Tendency of gel point reduction with NaCl.	41

Figure 31: Tendency of gel point reduction with Na ₂ SO ₄ .	42
Figure 32: Tendency of volume shrinkage for almost all samples (ex. CM) and the HM2Cl sample.	47
Figure 33: Exemplary adsorption isotherm of analyzed aerogel samples.	50
Figure 34: Pore size distribution C6288 samples.	52
Figure 35: Pore size distribution Sigmacell samples.	53
Figure 36: Pore size distribution hemp cellulose samples.	54
Figure 37: SEM images C6288: a) CM2Cl; b) CS2Cl.	56
Figure 38: SEM images Sigmacell: a) SM; b) SS.	57
Figure 39: SEM images hemp cellulose: a) HM2Cl; b) HS2Cl.	57
Figure 40: FTIR of milled hemp and hemp cellulose.	59
Figure 41: FTIR of milled hemp and hemp cellulose (zoom at area 1200-2000 cm ⁻¹).	60
Figure 42: FTIR of hemp cellulose and C6288 cellulose.	61

List of tables

Table 1: Synthesized cellulose solutions (For all tables: X = Used; - = Not used)....	24
Table 2: Steps during solvent exchange.	25
Table 3: Solutions, with added sodium salts, used for gel point analysis and monolith preparation.	29
Table 4: Samples used for envelope density analysis.....	29
Table 5: Samples for gas sorption measurements.	31
Table 6: SEM samples.	32
Table 7: Viscosity comparison of CaProLi cellulose solutions.....	36
Table 8: Gel point comparison of cellulose solutions without salt.....	38
Table 9: Gel point and storage modulus of the different cellulose CaProLi recipes.	40
Table 10: Abbreviations for aerogel samples.	43
Table 11: Skeletal density of cellulose.	43
Table 12: Envelope density of aerogel samples.....	44
Table 13: Porosity of aerogel samples.	45
Table 14: Shrinkage of aerogels samples (CaProLi recipe).	46
Table 15: BET surface area of monolithic aerogel samples.	49
Table 16: BET surface area of sheet shaped aerogel samples.....	49
Table 17: Average pore width and cumulative pore volume for monolithic aerogel samples.	55
Table 18: Average pore width and cumulative pore volume for aerogel sheet samples.	55

List of abbreviations and symbols

Abbreviation	Expansion of abbreviation
CaProLi	Cellulose Aerogel Production Line
CO ₂	Carbon Dioxide
DP	Degree of Polymerization
DMAc	N,N-Dimethylacetamide
FTIR	Fourier Transform Infrared Spectroscopy
IL	Ionic Liquid
KBr	Potassium Bromide
KOH	Potassium Hydroxide
LiCl	Lithium Chloride
N ₂	Nitrogen
NaCl	Sodium Chloride
NaOH	Sodium Hydroxide
Na ₂ SO ₄	Sodium Sulfate
NMMO	N-methylmorpholine-N-oxide
SEM	Scanning Electron Microscopy

Formula symbol	Name	Unit
C	Constant Gas Adsorption	-
G'	Storage Modulus	Pa
G''	Loss Modulus	Pa
N _A	Avogadro Constant	mol ⁻¹
P ₀	Atmospheric Pressure	bar
p ₁	Pressure Sample Chamber	bar
P ₂	Equilibrated Pressure	bar
r _{pore}	Pore Radius	m
S _{BET}	BET Surface Area (Specific)	m ² /g
S _{Gas}	Area Gas Molecule	m ²
V _{ads}	Volume Adsorbed Gas	m ³
V _C	Volume Sample Chamber	m ³
V _{Cylinder}	Cylindrical Volume	m ³
V _D	Dry Agent Volume	m ³
V _E	Volume Expansion Chamber	m ³
V _{mol,STP}	Molar Volume (0°C and 1bar)	m ³ /mol
V _{mono}	Volume Adsorbed Gas (Mono Layer)	m ³
V _s	Sample Volume	m ³
V _T	Total Volume	m ³
γ	Surface Tension	N/m
ρ _E	Envelope Density	g/cm ³
ρ _s	Skeletal Density	g/cm ³
Φ	Porosity	%

1. Introduction

Recently, there has been a growing interest in the production of bio-aerogels from natural polysaccharides due to large benefits in comparison to inorganic and organic aerogels. Polysaccharides, also known as biopolymers, are safe to use, have a high availability and are biodegradable. Cellulose is one of the most used polysaccharides when it comes to the production of aerogels.

The main sources for cellulose are from plant cell walls. To extract the cellulose from the plant cell walls, various steps have to be done, mainly to remove lignin and hemicellulose. Some outstanding properties of cellulose aerogels are low density ($0.005\text{-}0.35\text{ g/cm}^3$), high porosity (84-99.9 %) and large surface area ($10\text{-}975\text{ m}^2/\text{g}$) [1]. All the mentioned properties contribute to a highly insulating material ($0.03\text{-}0.04\text{ W/m}\cdot\text{K}$) [2]. Therefore, cellulose aerogels have the potential to replace common used heat insulation materials, such as mineral wool ($0.035\text{-}0.045\text{ W/m}\cdot\text{K}$) or expanded polystyrol ($0.035\text{-}0.040\text{ W/m}\cdot\text{K}$) [3]. Using cellulose aerogels as an insulating material could provide an environmentally friendly product and promote a more circular and bio-based building economy.

Based on this information, the aim of the work is to develop an upscaling process to manufacture cellulose insulation boards, using the CaProLi (**C**ellulose **A**erogel **P**roduction **L**ine). The insulation boards should be made of cellulose aerogel. The cellulose, which should be used for the board production, is extracted from hemp fibers. Hemp is a fast-growing herbaceous plant and therefore a very essential biomass resource. Hemp fibers are used in the textile industry (ex. clothes, ropes and bags) as well as in the production of bioplastics [4], but not all hemp fibers have the appropriate quality to be used for these processes. This “low quality” fibers are usually considered as waste. But these fibers can be an important resource for the cellulose aerogel production using the sodium hydroxide/urea/water pathway as solvent.

2. Literature review

2.1. Biomass

Biomass refers to a wide range of different bio-based resources from plants to animals, independent of being alive or dead. From the standpoint of bioenergy, biomass can be also defined as renewable resource of energy to use for the production of electricity and heat. These resources consist of biowastes, plant-based materials and aquatic organisms. As a renewable and sustainable energy resource, there is a constant biomass production by the interaction of CO₂, air, water, soil and sunlight. Using biomass for industrial applications has therefore a positive effect on the environment, such as reduced emissions, safer feedstocks and the promotion of a circular economy. According with the European committee for standardization, plants-based biomasses are divided into five groups (**Figure 1**) [5, 6]:

1. Woody biomass
2. Herbaceous biomass
3. Fruit biomass
4. Aquatic biomass
5. Blend and mixtures

Trees, shrubs and bushes fall under woody biomass, excluding their fruits or seeds. Herbaceous biomasses consist of plants which die at the end of the growing season, including its grains and cereals. The fruits belonging to the woody biomass resources make the fruit biomasses. The fourth category refers to plants that adapted to the life in or on aquatic environment. The last category includes blend and mixtures of biomasses which are created with or without intention respectively [5]. Vassilev proposed two additional categories, including animal and human waste and contaminated biomass [7].

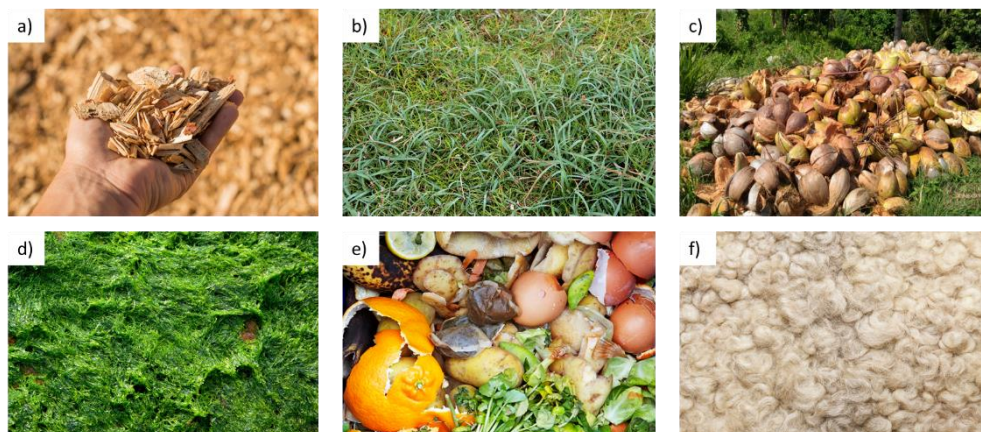


Figure 1: Examples for the different groups of biomasses: a) woody biomass, b) herbaceous biomass, c) fruit biomass, d) aquatic biomass, e) contaminated biomass, f) animal and human waste [8-13]

The usage of biomass can be divided into four major categories. These categories are chemicals, energy, electricity and transportation. There exist chemical (ex. extraction esterification), thermochemical (ex. pyrolysis) and biochemical (ex. digestion) processes regarding the conversion of biomass to energy and chemical products (**Figure 2**) [6].

One of the most interesting biomasses is hemp, due to its high sustainability properties and large utilization possibilities. Hemp is categorized as an oil crop and can be therefore used as source for biodiesel due to its high oil content as well as source for biomaterials due to its high cellulose content [14, 15].

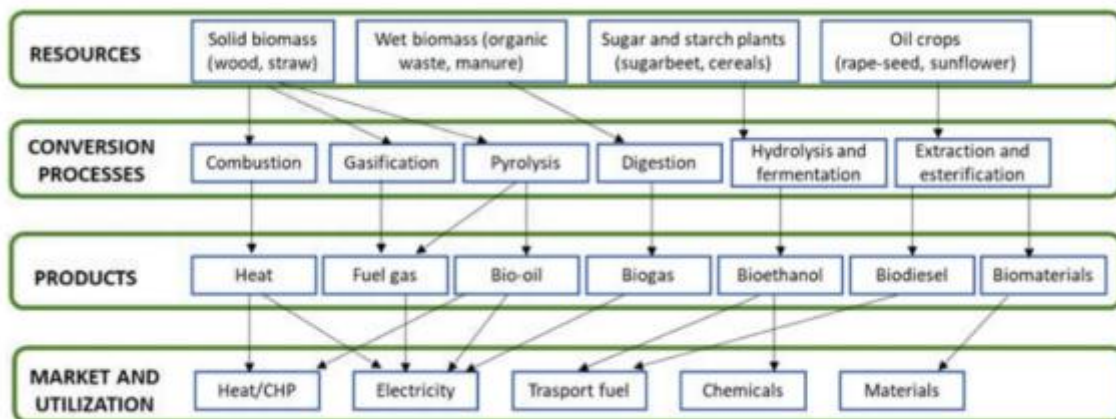


Figure 2: Usage categories of biomass [6].

2.2. Hemp

Hemp is an annual grown plant which is harvested to be used as a multipurpose crop. The different species of hemp are *Cannabis sativa* L, *Cannabis indica* L. and *Cannabis ruderalis*. Hemp has its origin from the Scythian folk. Traces of hemp were already discovered 8260 BC in Japan and the use of hemp as a textile reaches back to 6000 BC. Hemp is classified as a C3 crop, which grows most efficient in cooler and moist climates at higher temperatures, but the cultivation is not limited to temperate climate, although it grows best in these areas. There are around 47 countries cultivating hemp (**Figure 3**) of which the biggest producers are China, Russia, the USA, South Korea and Canada [16, 17]. In 2019 the hemp production in Europe was 152 kt [18]. Hemp is considered as very sustainable since it can take up to 22 tons of carbon per hectare and has excellent weed suppressing abilities. This provides a positive impact on biodiversity and in soil-cleaning. The five main parts of hemp are seeds, flowers, stem, roots and leaves. Every part of hemp is useful for different applications. The leaves are used in traditional medicine as a paste for wound healing. Seeds are used in the cosmetic and food industry due to the high oil content (28-35%). Roots are used for making medical tea. The stem is the most valuable part of the hemp plant, containing strong and ductile fibers. The fibers are used in the textile industry for example to produce clothes and ropes. Hemp fibers consists of 67% cellulose, 16.1% hemicellulose, 10% moisture, 3.3% lignin, 2.1% water-soluble, 0.8% pectins and 0.7% fat and wax. The high amount of cellulose in the hemp fibers makes them a promising source of cellulose [4, 17, 19, 20].



Figure 3: Hemp (left) and cultivating countries of hemp (right) [21, 22].

2.3. Cellulose

2.3.1. Overview

Cellulose is the most common biopolymer on earth. It was first discovered by the French chemist Anselme Payen in 1837 and it is distributed around Nature (**Figure 4**). It makes part of plants, algae, animals and fungi. However, the main source of cellulose is plant fiber. The cellulose acts as a structuring element in the architecture of plant cell walls. This leads to 40% of the carbon fractions in plants being cellulose. Cellulose can occur in plants but it is usually accompanied by hemicellulose, lignin and small amounts of other extractives [23, 24].

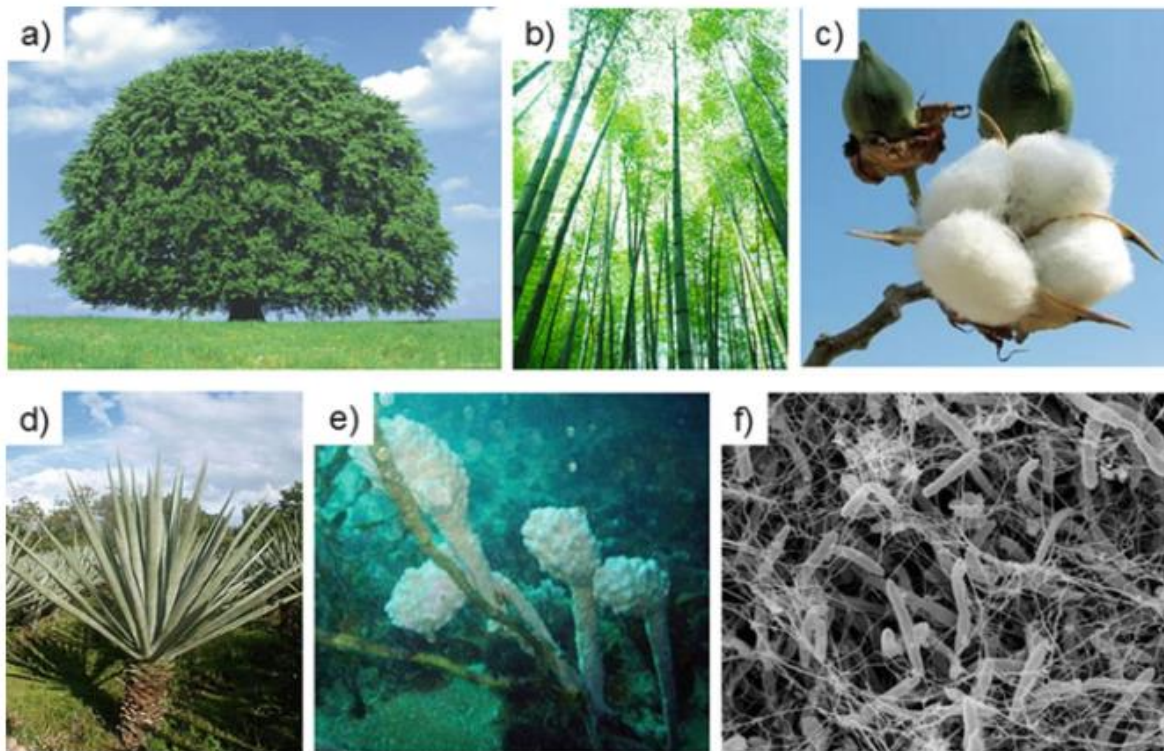


Figure 4: Important cellulose sources: a) hard wood (beech tree), b) bamboo, c) cotton, d) sisal, e) tunicine, and f) *Gluconacetobacter xylinum* [24].

Cellulose consists of D-glucopyranose ring units which are linked by β -1,4-glycosidic bonds causing an alternate turning of the cellulose axis by 180° (**Figure 5**). The repeating unit of cellulose is cellobiose with a length of 1.3 nm. Degree of polymerization (DP) values of native cellulose are in the range of 1000-30000 whereas extracted cellulose possesses a DP between 800-3000. The DP value represents an average value, because cellulose is a polydisperse substance. The molecular weight of extracted cellulose is 50000-500000 g/mol [24, 25].

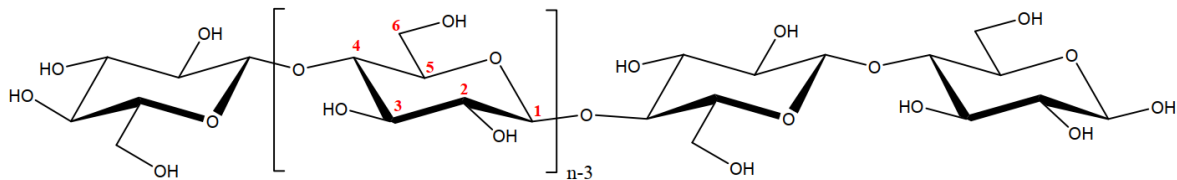


Figure 5: Structure of cellulose [26].

2.3.2. Morphology

The morphology of cellulose is composed of fibers with alternating crystal- and amorphous regions (**Figure 6**). The crystalline regions are ordered section of cellulose chains held together by van der Waals and hydrogen bonds while the amorphous regions are randomly arranged cellulose chains [27, 28]. Crystallinity of native cellulose is usually between 45-60%. The basic component of the cellulose fibers are the elementary fibrils with a length of 100 nm and a lateral dimension of 1.5-3.5 nm. Assimilation of such elementary fibers lead to microfibrils with a width of 10-30 nm that can also be assembled to microfibrillar bands (**Figure 6**). These microfibrillar bands have a width around 100 nm and a length of several hundred nanometers. These fibrillar architectures are characteristic for the cellulose fibers [24].

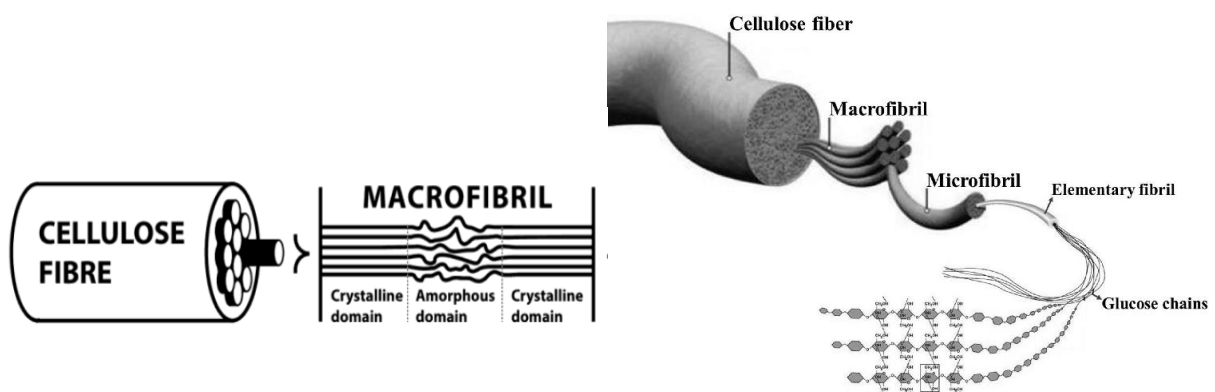


Figure 6: Morphology of cellulose: a) crystalline and amorphous structure in a macrofibril, b) elementary building blocks [29, 30].

The creation of several intra- and intermolecular hydrogen bonds has a significant effect on the properties of cellulose (**Figure 7**). The intramolecular hydrogen bonds are formed between the OH-group at C3 and the ether oxygen of the anhydroglucose units as well as between the oxygen at C6 and the OH-group at C2. Combined with the β -glycosidic covalent linkage the intramolecular hydrogen bonds are responsible for a rigid and stiff cellulose polymer chain. The intermolecular hydrogens bonds are formed between the oxygen atom at C3 and the OH-group at C6 of two neighbor cellulose chains leading to a limited solubility in most solvents and the crystalline structure of cellulose [24, 31].

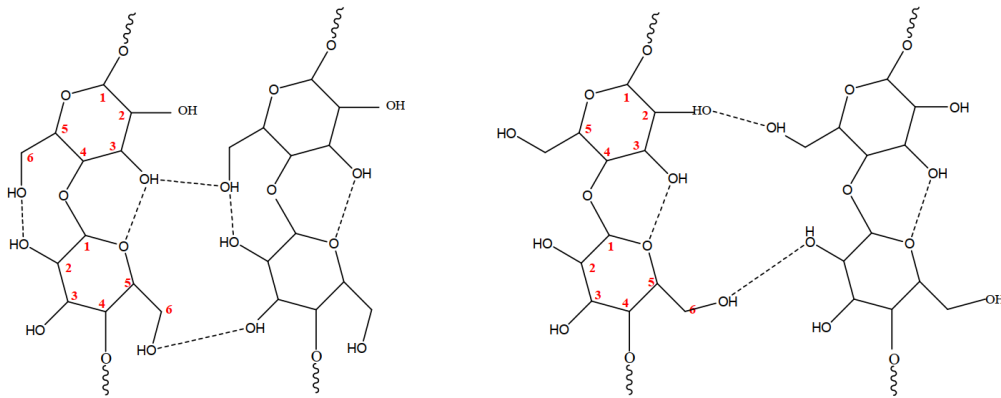


Figure 7: Hydrogen bonds in cellulose I (left) and cellulose II (right) [28].

2.3.3. Crystalline modifications

Different crystalline modifications are observed in cellulose depending on the applied treatment. Native cellulose has a crystalline cellulose I configuration. The crystalline formation of cellulose II can be achieved by regenerating cellulose I from the dissolved state or through its mercerization with a concentrated alkali solution (> 18 wt%). The difference between cellulose I and cellulose II is the orientation of the cellulose chains (**Figure 8**). While cellulose I has parallel oriented cellulose chains, the cellulose II has antiparallel oriented chains. This results in different intramolecular and intermolecular hydrogen bonds formations. Cellulose II has lower mechanical properties and a higher water absorbance in comparison to cellulose I. There are more crystal modifications of cellulose with cellulose III and cellulose IV that are achieved through chemical or thermal treatment but regarding the use of cellulose and its chemical derivatization only cellulose I and II are taken into consideration [24, 32, 33].

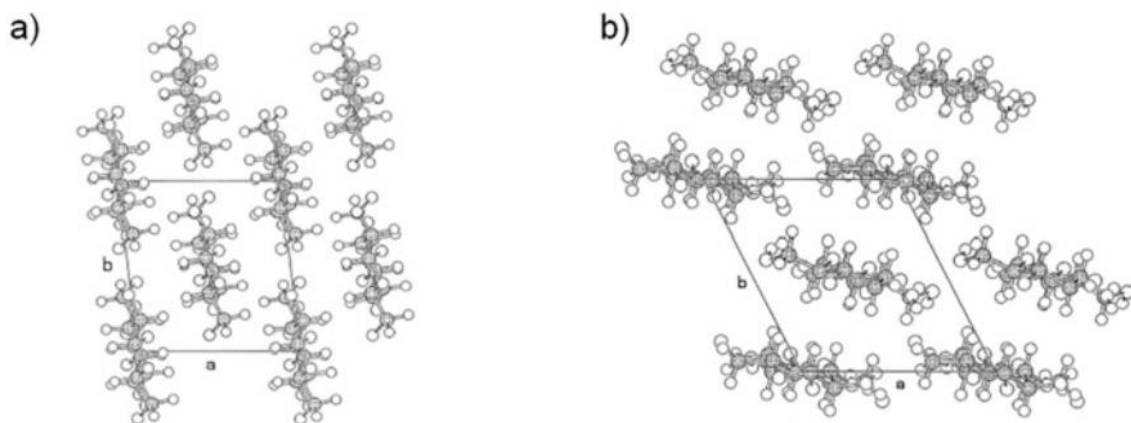


Figure 8: Crystal modification of cellulose: a) cellulose I, b) cellulose II [24]

2.4. Aerogels

Aerogels are ultralight materials with a very high porosity. The first aerogels were synthesized by S. S. Kistler in 1931 [34]. Kistler described aerogels as gels which are created by replacing the impregnated liquid with a gas while preventing the collapsing of the gel network [35]. The porosity of aerogel can reach 85-99.8%. Therefore, they can have a very high surface area (up to 1200 m²/g) as well as a very low density (< 0.2 g/cm³) and an extremely low thermal conductivity (< 2×10⁻² W/m×K) [36, 37]. Aerogels can be made of a variety of materials. In the literature, a broad range of aerogels achieved from different materials can be found, such as silica, alumina, carbon, metal oxides, resins and biopolymers [27]. There are some categories after aerogels can be classified, namely the appearance (monolith, powder or film), the difference in microstructural properties (microporous, mesoporous and mixed porous) or the composition [38] (**Figure 9**).

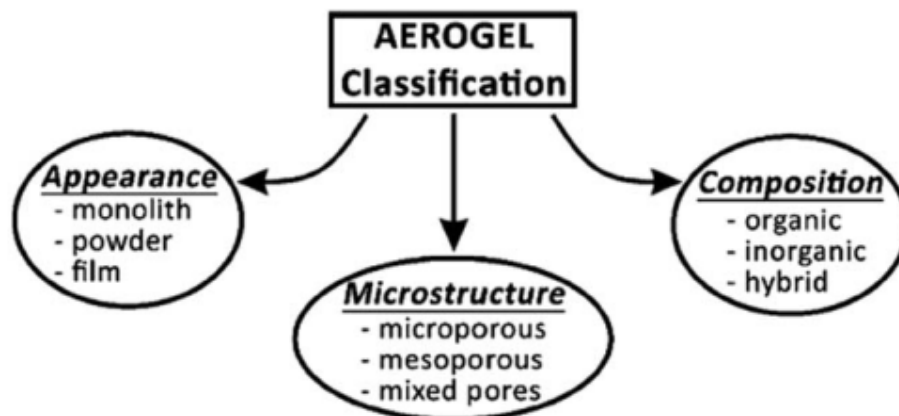


Figure 9: Aerogel Classification [38].

The preparation of aerogels follows generally a sol-gel synthesis. The first step is the creation of a colloidal solution followed by the gelation of the colloidal particles in the solvent. In the second step the solvent is exchanged, if needed, to form an organogel. The third step is the transformation of the organogel to an aerogel using supercritical drying or other drying techniques such as freeze drying. The benefit of using supercritical drying is that no capillary forces occur in the drying process which can cause a shrinkage and damage to the resulting aerogel. The reason for the elimination of capillary forces is the disappearing of the gas-liquid interface of a substance being in a supercritical state [27, 34, 38]. The procedure of making an aerogel changes depending on the material that is used. While the synthesis of inorganic and most organic aerogels starts often with polycondensation and/or hydrolysis of monomers, biopolymers are dissolved and the polymer chains rearrange during gelation. Some of

the most promising biopolymers used in aerogel synthesis are alginate, cellulose and chitin, with cellulose being the most abundant one [24, 39].

Looking at the function of aerogels they can be used in many application fields. Due to their unique properties' aerogels are used as thermal, electrical and sound insulators. Some other utilizations of aerogels are found as filters, storage systems for electrical energy or carriers of parenteral drug delivery systems [35].

2.5. Cellulose aerogels

2.5.1. Overview

Aerogels made of cellulose are flexible and highly porous. Their application fields are for example thermal superinsulation, tissue engineering and water filtering systems. The advantage of cellulose aerogels is the direct extraction from biomass without chemical modification [35]. The fine structure of cellulose aerogels can be controlled by several parameters, such as modification of building blocks, density, surface charge, coagulation bath composition, drying process and crosslinking agents. Furthermore, cellulose aerogels can be modified with inorganic materials to create a composite with specific properties [38].

2.5.2. Dissolution mechanisms

The first step in cellulose aerogel synthesis is the dissolution of cellulose in an appropriate medium by the disruption of the cellulose hydrogen bonding network. Several solvent systems were created to achieve a proper dissolution of cellulose. Some of them include amine oxides, such as N-methylmorpholine-N-oxide (NMMO), ionic liquids (IL), organic solvents in combination with inorganic salts like N,N-Dimethylacetamide (DMAc) with lithium chloride (LiCl) and aqueous solution of sodium hydroxide (NaOH)/NaOH-Urea watery solutions [38].

Dissolution of cellulose in NMMO happens by the interaction of the cellulose chains with the strongly dipolar N-oxide in NMMO which creates a hydrogen bond complex by disrupting the intra- and intermolecular hydrogen bonds in cellulose (**Figure 10**). The absence of water plays a significant role in the system, because water can interact with the oxygen atoms in NMMO. This prevents NMMO to create a complex with cellulose and therefore decreasing the dissolution capability of cellulose [38, 40].

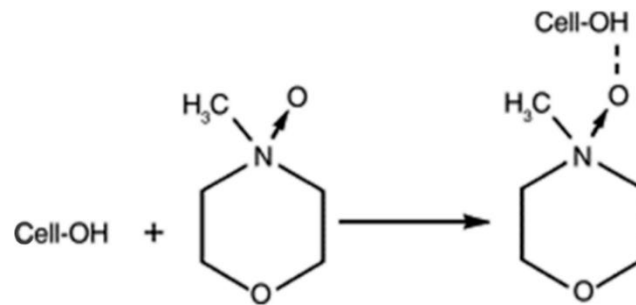


Figure 10: Dissolution Mechanism with NMMO [40].

Using IL as a solvation system for cellulose was first discovered by Rogers in 2002. IL are molten salts which are liquid up to 100°C due to the low vapor pressure resulted by the strong ionic interaction between the constituent ions. The dissolution mechanism of cellulose in IL happens mainly due to the interaction of the anion in the IL with the OH-groups of cellulose disrupting the inter- and intramolecular hydrogen bonds of the cellulose chains. Depending on the electron density of the anion the effect of the cellulose dissolution power is increased. Anions with a higher electron density have got a higher dissolution power. The most efficient anions in IL which are currently used are chloride, carboxylates, formate and propionate. Compared to the anions in IL, cations play a secondary role in cellulose dissolution only interacting over van der Waals forces with the cellulose chains. The most frequently used cations in IL are ammonium based, imidazolium-based, phosphonium-based and pyridinium-based. **Figure 11** shows a typical dissolution mechanism of an IL [40].

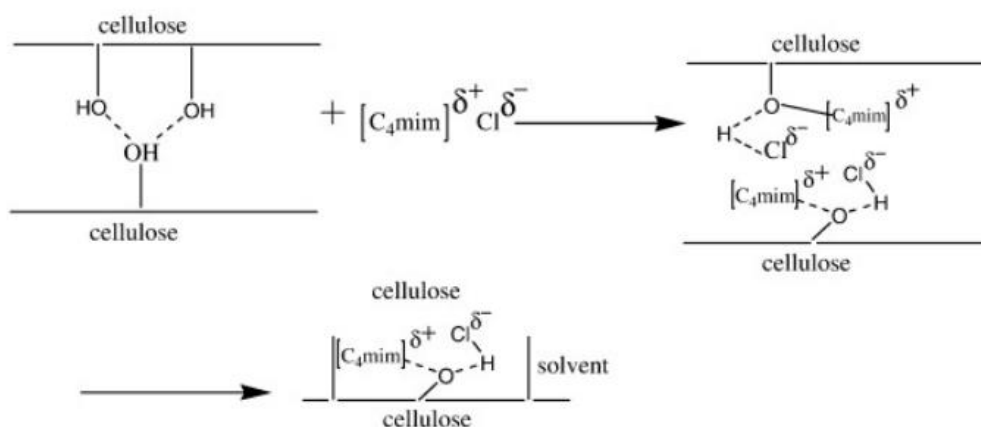


Figure 11: Dissolution mechanism with IL on the example of 1-butyl-3-methylimidazolium cation (C_4mim) and chloride [40].

DMAc and LiCl dissolve cellulose by building an interaction between the chloride ion of LiCl with the OH-groups of cellulose. The chloride ion is freed by the interaction of the lithium cation with the carbonyl group of DMAc (**Figure 12**). This results in the disruption of the hydrogen bonds between the cellulose chains [38].

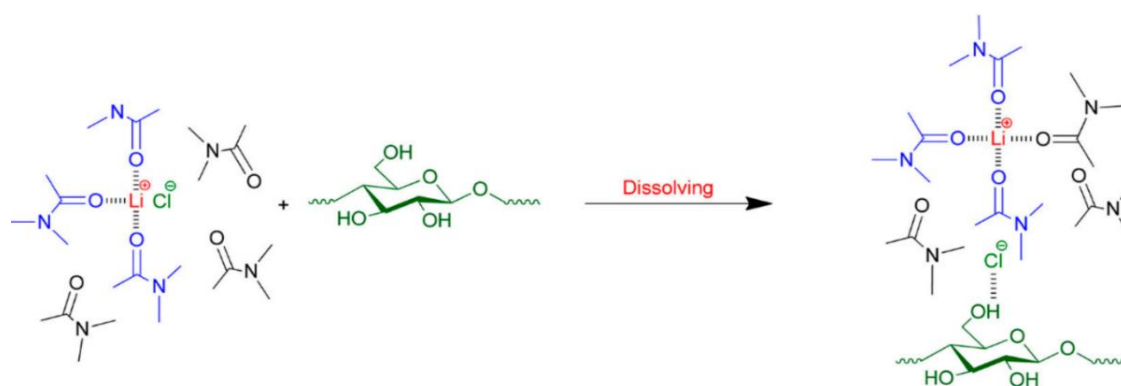


Figure 12: Dissolution mechanism with organic solvents in combination with inorganic salts on the example of N,N-Dimethylacetamide (DMAc) with lithium chloride (LiCl) [40].

The mechanism of cellulose dissolution in NaOH water solution is not yet fully understood. Different explanations have been proposed. A common understanding is that NaOH hydrates break the hydrogen bonds between the cellulose chains. **Figure 13** shows a schematic representation how the dissolution can look like on the example of cellobiose. The usage of NaOH/NaOH-Urea solutions to dissolve cellulose is limited to a concentration range of 7-10 wt% NaOH which can be explained by the concentration depended size of the NaOH hydrates. At low concentration the NaOH hydrates form a bigger hydrate shell that prevents the hydrates to penetrate the denser crystalline area of cellulose. Temperatures below 0°C are used for the dissolution with most researchers using a temperature between -12°C to -20°C to achieve a good dissolution of cellulose [40, 41]. Lower temperatures keep the solvent molecules arranged to stabilize the OH groups and the hydrophobic part in cellulose. The view on the effect of urea addition as an additive in the NaOH solution has several opinions. Xiong and Zhao explain that urea interacts with the hydrophobic part of the cellulose chains which is exposed when the NaOH hydrates break the hydrogen bonds between them. This interaction of urea with the hydrophobic part in cellulose leads to a reduction of hydrophobic interactions between the cellulose chains. At the same time the polar part of urea interacts with water which results in better dissolution [42].

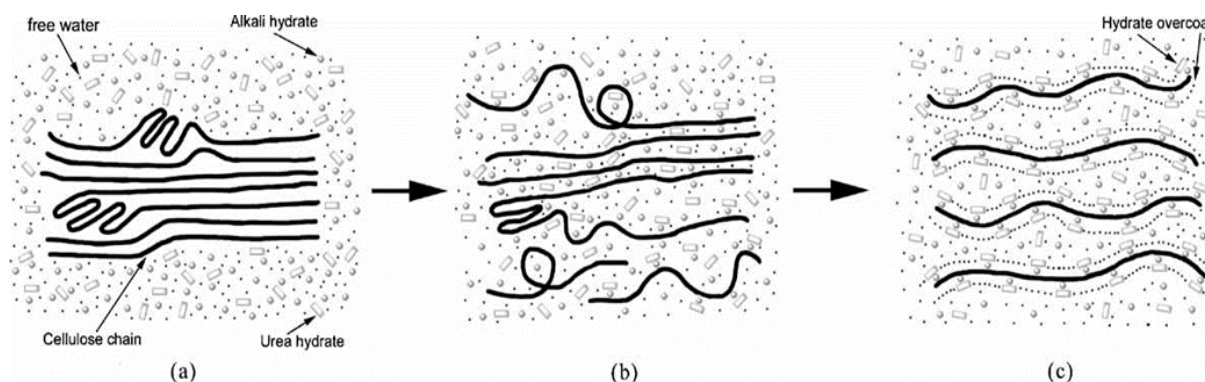


Figure 13: Process of cellulose dissolution with NaOH and Urea: a) cellulose bundle b) swollen cellulose c) dissolved cellulose [43].

2.5.3. Gelation mechanisms

After dissolution is achieved the cellulose is regenerated by the rearrangement of the polymer chains, causing gelation. There are many common ways to gel polysaccharides such as thermal treatment, changing the solvent pH value, anti-solvent induced phase separation (coagulation) and chemical crosslinking (**Figure 14**). For cellulose aerogels a common inducement of gelation is done with antisolvents, pH neutralization or thermal treatment. Furthermore, there exist some research to induce a faster gelation in cellulose solution using salts [44-46]. When gelation is achieved a solvent exchange is done for example with acetone or ethanol. In some ways of gelation, a neutralization with water may be needed before heading to solvent exchange. Finally, the cellulose gel is supercritical dried in CO₂ to obtain the cellulose aerogel [35, 39].

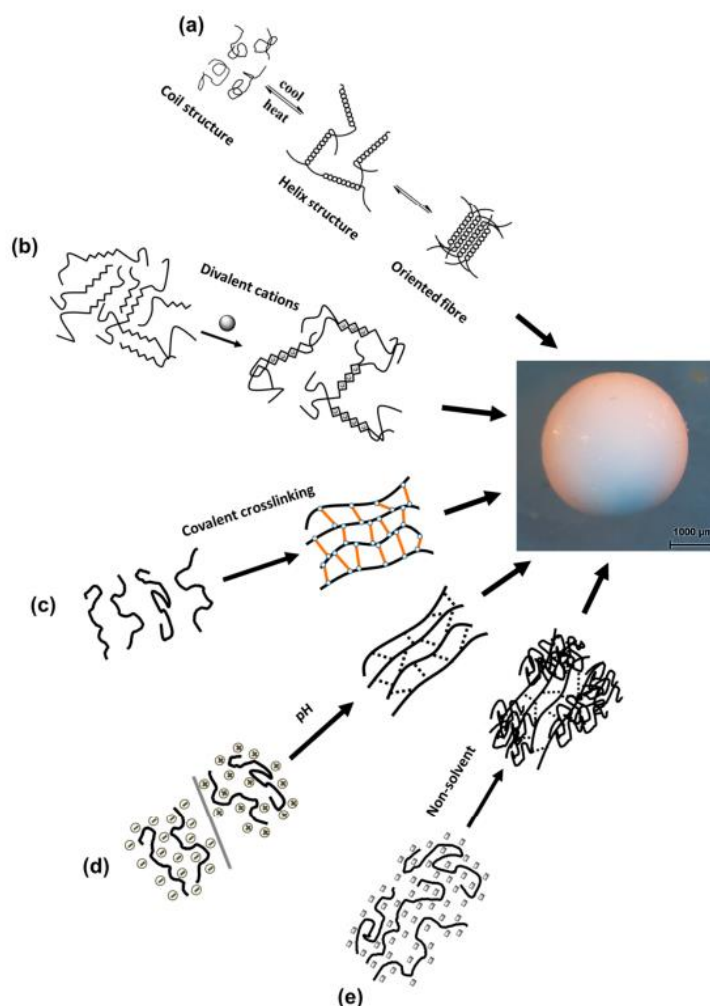


Figure 14: Common gelation mechanisms for polysaccharides: a) thermal treatment, b) ion-induced crosslinking, c) covalent crosslinking, d) pH-induced, e) anti-solvent [39].

3. Experimental part

3.1. Materials

For the research three different kinds of cellulose were used. Two of them are being commercially available and one is being extracted from hemp. The two commercially available cellulose were purchased from Sigma-Aldrich. The first commercial cellulose, product number C6288, is a medium fiber length and the second cellulose is called Sigmacell. Both celluloses from Sigma Aldrich were extracted from cotton-linters. The commercially available celluloses were used as references to obtain the right parameters for the upscaling production of the hemp cellulose board.

3.2. Methods

3.2.1. Rotational rheometry

Rotational rheometers are used to study the rheological properties of liquids. They consist of a fixed element (stator) and a rotating element (rotor). The liquid sample is placed between both elements which leads to shearing of the sample during operation. The sample can be subjected to a defined shear rate and shear stress that is achieved by the device knowing the rotational geometry as well as the force needed to cause rotation. Sample characterization can be done with a steady or oscillatory shear flow. Each flow is used to characterize different properties. Steady shear flow is mainly used for viscosity characterization over shear rate and time and oscillatory shear flow for the characterization of the viscoelastic properties. Three types of geometries are commonly used as rotational instruments, namely, cone and plate, concentric cylinder and parallel plate (**Figure 15**). Depending on the sample viscosity some geometries are better than others [47-49]. In this work a parallel plate setup is used.

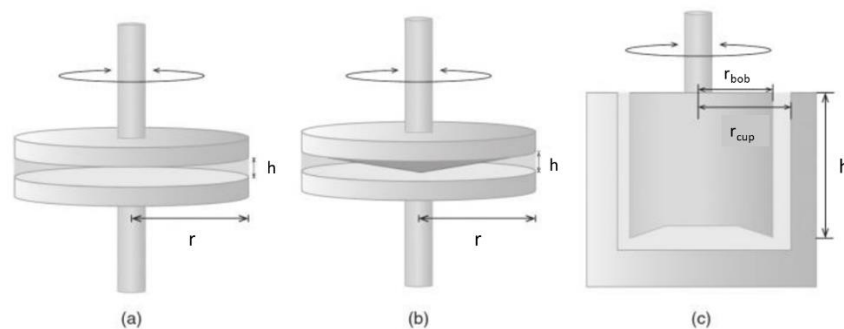


Figure 15: Commonly used geometries: a) parallel plate, b) cone and plate, c) concentric cylinder [50].

3.2.2. Gas pycnometry

A gas pycnometer is used for measuring the volume of a solid sample using the method of gas displacement applying the Boyle's law (Eq. 1). As a result of that, the skeletal density of the sample can be calculated using the ratio of mass to volume (Eq. 2). The volume measured in a gas pycnometer is the amount of space which is inaccessible to the gas. This leads to a result dependent on the atomic or molecular gas size. Helium is therefore commonly used as the gas medium because of its inertness and low atomic size [51]. A scheme of a gas pycnometer is shown in **Figure 16**.

To measure that inaccessible 3D space, the sample is placed inside a sample chamber with a pressure sensor and a known volume (V_C). Then, a first valve (valve A) is opened and the sample chamber, whose volume is reduced by the sample volume (V_S), is filled to a defined pressure (p_1). In the next step valve A is closed and a second valve (valve B) is opened. The gas, which was in the sample chamber, then enters the expansion chamber with a known volume (V_E) having atmospheric pressure (p_0). Next, the gas pycnometer waits until a constant pressure is achieved and record a pressure (p_2). Using Boyle's law, following equation is generated to calculate the V_S [52].

$$V_S = V_C - \frac{p_0 - p_2}{p_2 - p_1} \times V_E \quad (1)$$

$$\rho_s = \frac{m}{V_S} \quad (2)$$

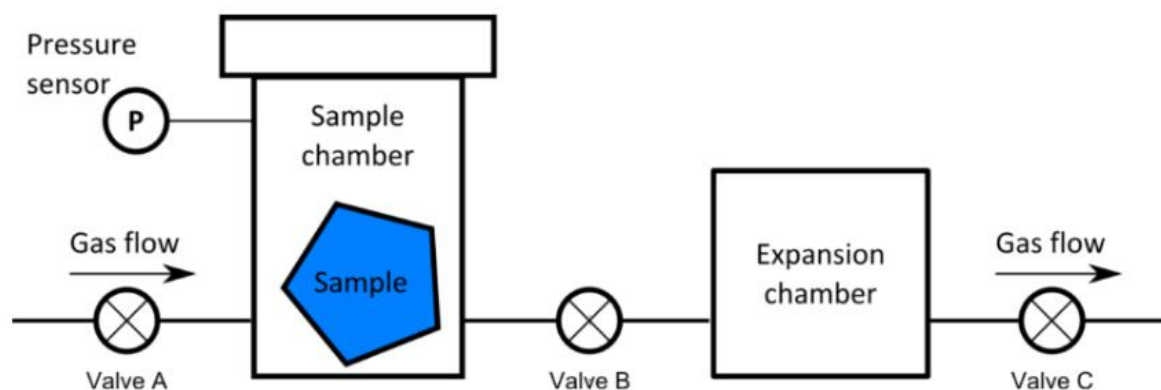


Figure 16: Setup gas pycnometer [52].

3.2.3. Quasi-fluid pycnometry

Quasi-fluid pycnometers measure the volume of a sample using a dry agent, instead of a liquid to analyze the sample density. It is a modification of liquid pycnometry with the advantage that it eliminates the wetting phenomenon. This advantage is used to measure very absorptive materials. In comparison to gas pycnometers, fluid- and quasi-fluid pycnometers have higher density errors because of the inability of the agent to permeate pores. Therefore, quasi-fluid pycnometry is mainly used for envelope density determination additionally entering the sample mass in the device [53, 54].

The analysis starts by first measuring the volume of the dry agent placed in a cylindrical chamber of known diameter (Step A). This happens by the distance a piston penetrates the chamber, while compressing the powder. Then the sample is placed in the chamber and the total volume is determined with the same procedure (Step B). The sample volume (V_S) is then determined by the difference between the total volume (V_T) and the dry agent volume (V_D) (Eq. 3). After that, the envelope density can be calculated over mass to volume ratio (Eq. 4) [53, 54]. The process of operation is shown in **Figure 17**.

$$V_S = \left(\left(\frac{d}{2} \right)^2 \times \pi \right) \times \Delta h = V_T - V_D \quad (3)$$

$$\rho_s = \frac{m}{V_S} \quad (4)$$

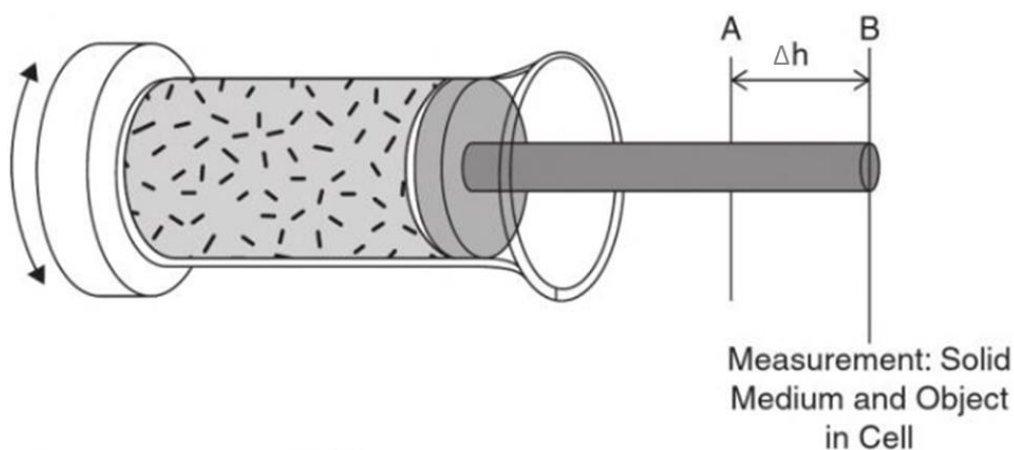


Figure 17: Setup quasi-fluid pycnometer [55].

3.2.4. Gas sorption method

The gas sorption measurement analyses the interaction between a gas (adsorptive) and a solid sample (adsorbent). The interaction can occur in several ways:

1. Adsorption in pores of different sizes (micropores, mesopores or macropores)
2. Mono- and multilayer adsorption
3. Liquid/Solid interaction

The most commonly used technique is N₂ sorption at -196°C. By increasing the pressure from vacuum to ambient pressure (1 bar) and vice versa the adsorbed amount of gas on the sample can be detected over several relative gas pressures (p/p_0). This results in an adsorption isotherm, which assumes that the system consisting of adsorbent, adsorptive and adsorbate is in equilibrium at each point taken. Adsorption isotherms give information on the specific surface area and the pore size distribution of the sample. Recording an isotherm implies that the sample has to be well degassed and evacuated to prevent interaction with other substances. Adsorption isotherms can be divided into five different types describing different morphological conditions (**Figure 18**). Type IV isotherms are typical for aerogels [35].

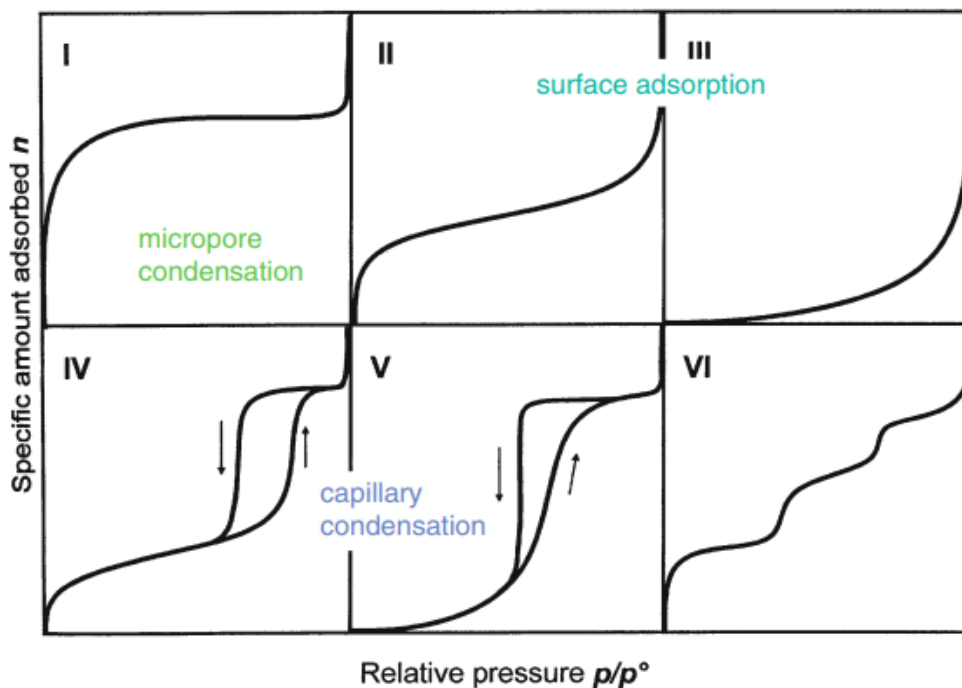


Figure 18: Different adsorption-desorption isotherms [35].

The most universally used method for surface area determination is the BET method provided by Brunauer, Emmett and Teller in the late 1930s. The BET method describes the adsorption of molecules on a sample surface in multiple layers as a function of the relative pressures of the adsorbate in the gas phase. Nevertheless, the model has the strong assumption that the layers after the monolayer do not interact with the sample surface. For an infinite number of possible layers, the amount of adsorbed gas (V_{ads}) can be calculated with Eq. 5 [35, 56, 57]:

$$\frac{p/p_0}{V_{ads} \times (1 - p/p_0)} = \underbrace{\frac{1}{V_{mono} \times C}}_b + \underbrace{\frac{C - 1}{V_{mono} \times C}}_m \times (p/p_0) \quad (5)$$

This equation is valid for relative pressures from 0,05-0,30. The amount of gas which covers the monolayer corresponds to V_{mono} . The parameter C describes the adsorption behavior of the gas molecules on the monolayer. Term b represents the ordinate and term m the slope of the equation. With that the parameters C and V_{mono} can be calculated as followed [35, 57]:

$$C = \frac{m}{b} \quad (6)$$

$$V_{mono} = 1/(b + m) \quad (7)$$

Knowing V_{mono} and C , the BET surface area (S_{BET}) can be determined with following equation [35]:

$$S_{BET} = \frac{V_{mono} \times S_{Gas} \times N_A}{V_{mol,STP}} \quad (8)$$

S_{Gas} represents the area taken by a single adsorbate molecule (0.162 nm² for N₂), N_A is the Avogadro constant and $V_{mol,STP}$ the molar volume (22.414 cm³) at a standard temperature of 0°C and atmospheric pressure [35].

The most widely used approach to get a pore size distribution from an adsorption isotherm is the BJH method by **B**arrett; **J**oyner and **H**alenda. This method is based on the capillary condensation in mesoporous sorbents. For application the desorption branch of the isotherm is used. It is assumed that there are only cylindrical pores. Pore size distribution is calculated with the simple Kelvin equation (Eq. 9) with the pore radius being r_{pore} and γ being the surface tension [35, 58]:

$$\ln\left(\frac{p}{p_0}\right) = \frac{2 \times \gamma \times V_{mol,STP}}{r_{pore} \times R \times T} \quad (9)$$

3.2.5. Scanning electron microscopy (SEM)

SEM uses a very extremely focused primary electron beam directed to a sample to achieve high-resolution imaging of it. Resolutions up to 1 nm can be achieved in that way. To accelerate the electrons a maximum voltage of up to 30 keV is applied. Depending on acceleration voltage the electrons can penetrate deeper into the sample providing a deeper imaging of it. For the sample to be analyzed it has to be well conductive, otherwise charges are accumulated on the sample. This results in an electric field that interferes with the imaging system in the microscope. To prevent that, non-conductive samples are coated with a layer of a few nanometers consisting of gold and palladium or carbon. The image creation is based on the emission of electrons and X-rays from the sample to detectors (**Figure 19**). There are two types of emitted electrons. Secondary electrons (SE) are emitted from the upper layer of a sample from a depth of less than 50 nm or equivalent. SE are inelastic scattered electrons emitted by the sample. Backscattered electrons (BSE) are electrons of deeper areas in the sample that are elastically. The BSE signal can be also used to image the local distribution of elements. X-Rays are emitted through inelastic interaction of the outer shell electrons within the sample with SE and BSE. By using an energy dispersive detector, the elementary composition of the sample can be analyzed as well Handbook [35].

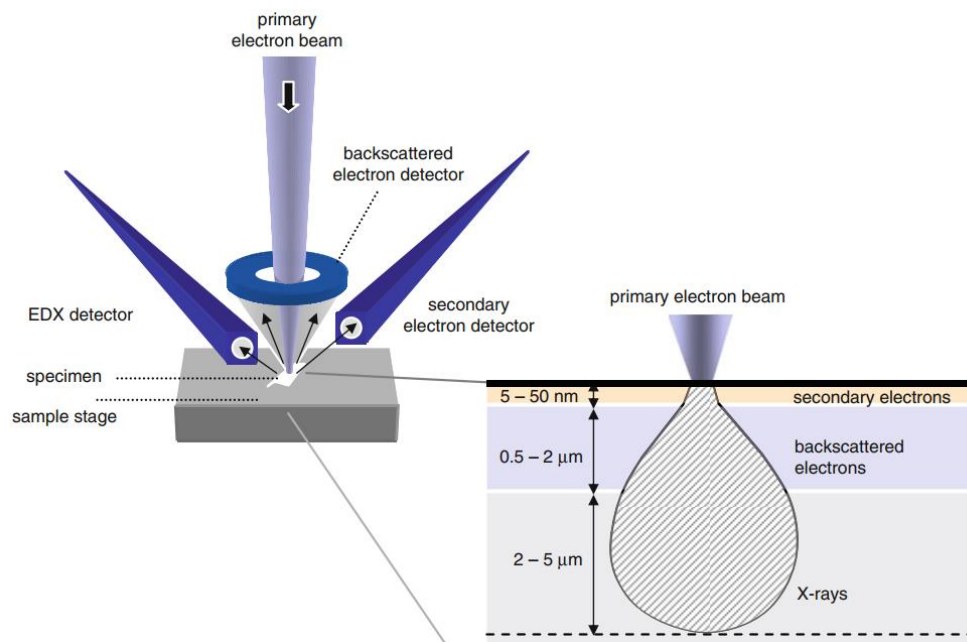


Figure 19: SEM functionality (left) and penetration depth of different picture generating sources (right.) [35]

3.2.6. Fourier transform infrared spectroscopy (FTIR)

FTIR is a modified technology of infrared spectroscopy (IR), which is more sensitive and faster. IR uses the interaction of certain molecules with infrared radiation. The molecules absorb energy at certain wavelengths of the infrared radiation, while being excited to a higher vibrational state. The absorbed energies correspond to the vibration frequencies between the atomic bonds. The resultant spectrum shows the molecular absorption and transmission of the infrared radiation. This leads to the generation of an infrared spectrum with a unique fingerprint, depended of the material composition [59].

Standard IR has the big disadvantage that the spectra are measured sequentially, meaning that the spectrometer is tuned through a range of wavelengths, while the detector registers the absorption of radiation over time. This takes a lot of time since the absorption lines are typically narrow. FTIR overcomes this problem by analyzing the whole spectrum at once, using an interferometer (**Figure 20**) [60]. In the interferometer the infrared radiation passes through a mirror called “beam splitter”, which separates the incoming radiation into two perpendicular beams. One beam is undeflected and the other is oriented at a 90° angle. The beam oriented at a 90° angle goes to a fixed mirror and is returned to the beam splitter and the undeflected beam goes to a moving mirror and is also returned to the beam splitter. The moving mirror causes a variation of the pathlength. When both beams recombine at the beam splitter, their pathlength differs, causing constructive and destructive interferences. This combined beam is called the interferogram and contains all the radiative energy coming from the source and has a wide range of wavelengths. The interferogram is then oriented to the sample and the sample simultaneously absorbs all wavelengths that are found in infrared spectrum. Liquid samples are usually put between two salt plates made of sodium chloride (NaCl) or potassium bromide (KBr) and solid samples are pressed with KBr to a pellet. As NaCl and KBr are ionic substances they do not absorb infrared radiation. After the interferogram passes the sample and reaches the detector, it contains information about the amount of energy that was absorbed at every wavelength. Finally, a computer extracts the information to produce a typical infrared spectrum, using Fourier transformation [61].

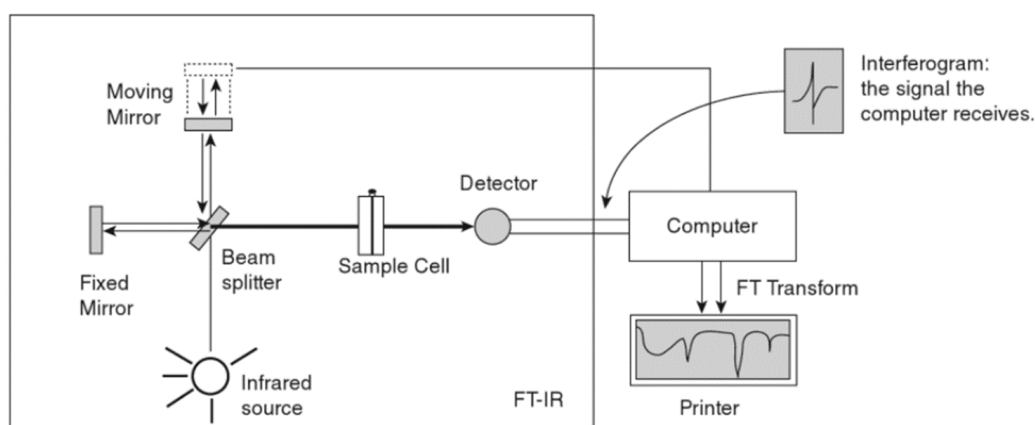


Figure 20: FTIR setup [61].

3.3. Extraction of cellulose and synthesis of aerogels

3.3.1. Grinding of hemp fibers

To extract the cellulose out of the hemp fibers they were first milled (**Figure 21**) with the SR200 rotor beater mill by Retsch®. Milling is done to achieve a higher yield of extracted cellulose due to the generation of a higher surface area [62]. Before starting the milling process, the fibers were cut to a length of ~2 cm. liquid N₂ was used to refrigerate the machine and fibers in order to prevent the fibers of getting softer which would hinder the milling process. Therefore, liquid nitrogen was poured every 5 min into the mill.

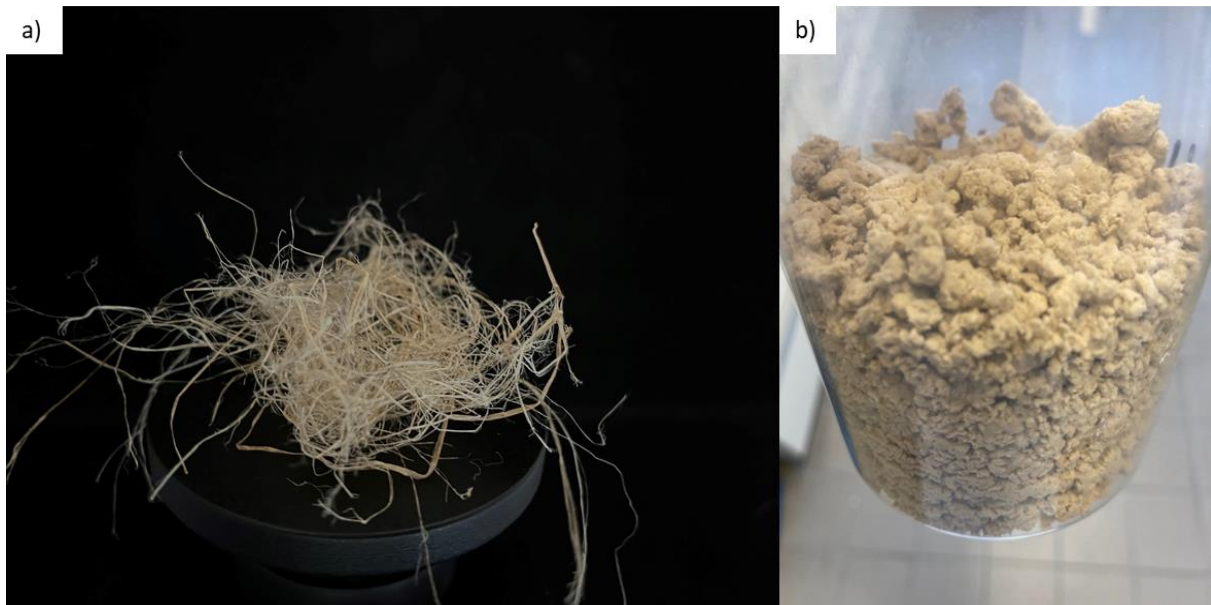


Figure 21: Hemp fibers (left) and grinded hemp fibers (right).

3.3.2. Cellulose extraction

For the extraction of cellulose from the milled hemp fibers two steps are needed. First, the alkali treatment in NaOH solution to remove hemicellulose and some percentage of lignin and secondly the bleaching to remove the lignin completely [63].

Step 1: The alkali treatment was done in a round bottom flask containing 900 g of NaOH-solution (8wt% NaOH). 50 g of milled hemp fibers were added into the flask and left stand overnight under stirring. On the next day the mixture was heated at 60°C for 3 hours under stirring. After cooling to room temperature, the mixture was neutralized, using acetic acid (glacial). Next, the fibers were collected by filtration in a sieve (100 µm] and washed five times with 500 ml of distilled water. Then they were washed with 500 ml of ethanol and 100 ml of acetone. Finally, the fibers were dried in a vacuum oven at 50°C over night (**Figure 22**).

Step 2: Afterwards the fibers were taken out of the oven to start the bleaching process. Therefore, the fibers were taken in a round bottom flask containing 900 g of potassium hydroxide (KOH) solution (5 wt% KOH) and stirred until dispersion. Furthermore, 45 ml of hydrogen peroxide in water (30%) was added to the mixture and stirred. Then the mixture was left to stand overnight. On the next day the mixture was neutralized with acetic acid (glacial) and the fibers were filtered in a sieve (100 µm). Finally, the fibers were washed and dried with the same procedure as in the alkali treatment step (**Figure 22**). The yield of the pure cellulose was around 70%.



Figure 22: Dried alkalization product (left) and dried cellulose after bleaching (right)

3.3.3. Solution preparation

To prepare the cellulose solution for the aerogel synthesis 14 g of NaOH were added to cup with 162 g of distilled water while stirring. The cup was in a water bath to cool it during the exothermal reaction while adding NaOH. The solution was stirred until the NaOH was fully dissolved and the cup reached room temperature. After that, different amounts of cellulose were added to the solution (**Table 1**) to achieve later a certain cellulose solution concentration. The solution was stirred for an additional 15 min to achieve a good dispersion of the cellulose fibers while being out of the water bath. Then the solution was put in an ice bath for 1 hour while stirring to start the dissolution process. After 1 hour 24 g of urea were added to the cellulose solution and the solution was then stirred for an additional hour. Following this step, the solution was taken out of the ice bath and stirred for 15 min at room temperature and then stored in the freezer at -20°C overnight.

Table 1: Synthesized cellulose solutions (For all tables: X = Used; - = Not used).

Solution	3 wt%	5 wt%	7 wt%	9 wt%
C6288	-	X	X	X
Sigmacell	-	-	X	-
Hemp	X	X	-	-

3.3.4. Monolith preparation

For the preparation of the aerogel monoliths, the cellulose solutions were taken out of the freezer and thawed under room temperature. After reaching room temperature, the cellulose solutions were stirred for 1 hour to get homogenous. Then each solution was transferred into 4 cylindrical containers (d=3.1 cm) to achieve the monolithic shape. Some monoliths were also prepared with the addition of two different sodium salts (**Table 3**). In that case, the salt was added into the homogeneous cellulose solution and stirred until fully dissolved before transferring the solution into the containers. The containers were filled 2 cm high with solution. Next, the containers were stored at 50°C for 30 minutes in the oven to obtain a weak gel network. If some containers happened to have solution with air bubbles, before storing them in the oven, they were first centrifugated at 1000 rpm for 5 min. Removing of air bubbles will prevent bigger voids in the monolithic aerogel which would weaken the properties. After storing the containers in the oven, they were left standing at room temperature over night. On the following day a gelation bath was prepared consisting of 90 wt% ethanol and 10 wt%

acetic acid, in which the containers were stored in for two additional days to form the gel body.

The next step was the washing and neutralization of the gel bodies with distilled water. Therefore, the gel bodies were washed 5 times with 500 ml of distilled water. Next, a solvent exchange from water to ethanol was done to prepare the gels for supercritical drying. Water is not mixable with supercritical CO₂ to dry the gels. The solvent exchange was done in five steps (**Table 2**) to prevent pore collapsing. The final step is to dry the alcogels in an autoclave with supercritical CO₂ to get the aerogels (**Figure 23**).

Table 2: Steps during solvent exchange.

Step	Volume ratio (water/ethanol)
1	80/20
2	60/40
3	40/60
4	20/80
5	0/100



Figure 23: Cellulose aerogel monolith.

3.3.5. Sheet preparation

The solutions for the aerogel sheet preparation are proceeded the same way as the cellulose solutions for monoliths in chapter 3.3.4. until the homogenization. After the cellulose solution is homogenized, the gel sheets are directly made with a special device called CaProLi (**Figure 24**). Part of solutions are tested by adding sodium salts. Therefore, the salt has to be fully dissolved in the solution, before being used in the CaProLi device.

This device was constructed by the DLR with the intention to be used for aerogel sheet production. It mainly consists of a conveyor belt, three flattening rolls, a mixing unit connected to a slit die and a cutting wheel. In this work, only the conveyor belt and the flattening rolls are used to prepare the aerogel sheets. The time for the solution to become a stable gel body is ~140 s at the lowest velocity of the belt. In the first step, the gel solution is poured over the belt at the height where the solution would normally come out of the slit die. Then the cellulose solution is distributed evenly with a dough scraper. Next, the engine of the conveyor belt is started and the solution is transported to the first flattening roll. The first flattening roll defines the thickness of the sheets and has a gap of ~0.3 mm. After the cellulose solution is flattened by the first roll to the defined thickness, a mixture consisting of 80 wt% ethanol and 20 wt% lactic acid is constantly sprayed over the cellulose solution/gel body until the end of the conveyor belt. This mixture is used as a gelation medium to replace the mixture used as a gelation bath in the monolith preparation. The advantage of lactic acid in comparison to acidic acid is that there is less evaporation while spraying during sheet production on, as well is in higher acidity increasing the gelation velocity. The higher amount of the acid part (20 wt%) used in this chapter, additionally increases the gelation velocity to achieve a stronger gel body at the end of the conveyor belt. The second and third flattening rolls are used as wetting rolls to help distribute the gelation medium over the weak gel body of the sheet.

After reaching the end of the conveyor belt the gel body in sheet form is cut with a scalpel in several parts to be transferred into a box with distilled water, that is used as a washing and neutralization bath. Then the same procedure as in the previous chapter is done to prepare the sheets for the supercritical drying with CO₂ (**Figure 25**).



Figure 24: Setup CaProLi for sheet production.



Figure 25: Cellulose aerogel sheet.

3.4. Measurements

3.4.1. Viscosity

The viscosity of the three different cellulose solutions was investigated with the Haake™ Mars™ 60 rheometer by Thermo Scientific™. The measurements were done with a steady shear rate from 1-1000 1/s using a gap of 0.8 mm. A plate-plate geometry with a diameter of 35 mm made of titanium was utilized. The viscosity values at a shear rate of 1000 1/s were taken to compare the solutions.

Taking into account the limited resource of hemp fibers to extract the hemp cellulose, the measurements were first done with the commercial cellulose C6288, using it as a reference cellulose solution. The aim was to find a solution with the appropriate viscosity to obtain a good shape and faster gelation. Therefore, three different concentrations were used (**Table 3**). Later, a viscosity measurement of the Sigmacell cellulose solution was done, considering the proper cellulose concentration which was chosen before. The reason behind the usage of the Sigmacell cellulose was to have a second reference solution to adapt a proper hemp cellulose solution for the cellulose board upscaling process. Based on the obtained results of the reference cellulose solutions, two hemp cellulose solutions with different cellulose concentration were analyzed. The reason behind the synthesizing of the different hemp cellulose solutions was to find a viscosity close to the reference solutions.

3.4.2. Gel point

Gel point measurements were also done with the Haake™ Mars™ 60 rheometer using a plate-plate geometry with a diameter of 35 mm made of titanium. The measurements were done with an oscillating frequency of 1 Hz and a gap of 0.8 mm. The gel point is defined as the point of incipient chemical or physical polymer network formation, meaning it is the point where a gel starts to form. The gel point is identified as the point where the storage modulus G' becomes larger than the loss modulus G'' . G' representing the elastic behavior of the solution and G'' the viscous behavior.

The proper cellulose concentrations of chapter 2.3 were used for the several solutions. The goal was to analyze the time needed for the cellulose solutions to gel, considering that there was a limited amount of time to obtain a stable gel body during the production on the CaProLi device. In some samples, additional sodium salts were added (**Table 3**) to analyze the influence on the gel point. For the preparation of these samples 20 g of cellulose solution was used and stirred after salt addition for 5 min.

Table 3: Solutions, with added sodium salts, used for gel point analysis and monolith preparation.

Samples	NaCl		Na ₂ SO ₄	
	1 wt%	2 wt%	1 wt%	2 wt%
C6288	X	X	X	X
Hemp	-	X	-	-

3.4.3. Densities and porosity

Skeletal density

The skeletal density was measured with the AccuPyc II 1340 by Micrometrics. For the measurement a part of a cellulose aerogel monolith was finely crushed in a mortar and filled in the sample container being then compressed. The sample mass was measured beforehand. The volume of the sample was about 70% of the sample container. Helium was used as the inert gas. The density was measured 10 times in one measurement. Three measurements were done in this way.

Envelope density

The envelope density of the cellulose aerogel monoliths was measured with the Geopyc™ 1360 by Micrometrics using DryFlow™ as the enclosing medium around the sample. The precision cylinder used as a sample cell was filled with DryFlow™ up to 2.5 cm. The volume of a sample was around 25 % compared to the DryFlow™ amount. 51 N of force were applied during the measurement. The envelope density was measured 10 times during one measurement. This procedure was done 3 times for every monolith type. **Table 4** shows the analyzed samples.

Table 4: Samples used for envelope density analysis.

Monolith	No Salt	NaCl		Na ₂ SO ₄	
		1 wt%	2 wt%	1 wt%	2 wt%
C6288	X	X	X	X	X
Sigmacell	X	-	-	-	-
Hemp	X	-	X	-	-

Porosity

To calculate the porosity of every sample used in **Table 3**, following equation was used:

$$\phi = \left(1 - \frac{\rho_e}{\rho_s}\right) \times 100\% \quad (10)$$

3.4.4. Volume shrinkage

For the volume shrinkage determination of the different monolith types (**Table 3**) following states were analyzed:

1. Hydrogel
2. Alcogel
3. Aerogel

The volume was calculated by measuring the height and the diameter using the equation for a cylindrical volume:

$$V_{cylinder} = \left(\left(\frac{d}{2}\right)^2 \times \pi\right) \times h \quad (11)$$

For the calculation of the shrinkage (in %) the solution volume in the container was taken as the reference. The volume calculation was done with 3 samples of every monolith type.

3.4.5. Surface and pore size distribution

For gas sorption measurements the TriStar™ II 3020 device by Micrometrics was used. The analyses were done with N₂ as the adsorptive medium using 62 measuring points. During the analysis the samples were cooled in a liquid nitrogen bath. Before analyzing the samples (**Table 5**) with the TriStar™ II 3020 they were vacuum dried with the VacPrep™ 061 by Micrometrics at 110°C over night to make sure that the samples didn't contain water. All samples were measured 3 times. The BET method was used to determine the surface area and the BJH method was used for the analysis of the pore size distribution.

Table 5: Samples for gas sorption measurements.

Geometry	Samples	No Salt	NaCl		Na ₂ SO ₄	
			1 wt%	2 wt%	1 wt%	2 wt%
	C6288	X	X	X	X	X
Monolithic	Sigmacell	X	-	-	-	-
	Hemp	X	-	X	-	-
	C6288	-	-	X	-	-
Sheet	Sigmacell	X	-	-	-	-
	Hemp	X	-	X	-	-

3.4.6. Morphology

To investigate the morphology of the samples, scanning electron microscope (SEM) image analyses were done using an Ultra 55 microscope by Zeiss. For sample preparation a part of the sample was put on a sample holder which had a carbon adhesive pad on it. Then the sample was coated for 90 s with platinum using an SCD 500 sputter coater by BAL-TEC. The current used during coating was 21 mA and the pressure 4×10^{-2} mbar. For the SEM analyses a voltage of 3 kV was used with a working distance of 6.5-7.8 mm. **Table 6** shows the analyzed samples.

Table 6: SEM samples.

		NaCl	
Geometry	Samples	No Salt	2 wt%
	C6288 Cellulose	X	X
Monolithic	Sigmacell	X	-
	Hemp	X	X
	C6288 Cellulose	-	X
Sheet	Sigmacell	X	-
	Hemp	-	X

3.4.7. FTIR

The FTIR analysis of hemp fibers, hemp cellulose and C6288 cellulose was done with the Bruker Tensor 27. Each sample was crushed and mixed with KBr in mortar. Next, the mixture was pressed to a pellet under pressure to be used in the FTIR. The FTIR measurement was done with a resolution of 4 cm^{-1} and 80 scans. The analyzed area was $400\text{-}4000 \text{ cm}^{-1}$. The aim was to prove that the extracted hemp cellulose had no impurities.

4. Results and discussion

4.1. Viscosity

4.1.1. C6288 cellulose

Representative viscosity curves of the different cellulose solution made with C6288 are shown in **Figure 26**. At a shearing rate of 1000/s, the 9 wt% cellulose solution has the highest viscosity (0.83 Pa·s), followed by the 7 wt% cellulose solution (0.39 Pa·s). The 5 wt% cellulose solution has the lowest viscosity (0.16 Pa·s). Decrease of viscosity is observed for all solutions while being exposed to higher shear rates. This effect is stronger in the beginning as shown by the viscosity of the cellulose solution with 9 wt% of C6288 cellulose. Looking at higher shear rates, the decrease of viscosity is slower and the viscosity seems to asymptotic approach a final value.

The reason for the decrease of viscosity while shearing is the orientation of the cellulose chains and the existence of inter- and intramolecular interactions between molecules in the cellulose solution. Before being exposed to shearing the cellulose chains are entangled and have a stronger interaction with each other, which results in a higher viscosity. Once a shear rate is applied, the cellulose chains start to get disentangled and the interaction between the cellulose chains is reduced. This is characteristic for polymeric solutions and is called shear thinning [64].

The cellulose solution with 7 wt% of the C6288 cellulose has the appropriate viscosity for the upscaling process with the CaProLi device as it is viscous enough to maintain its shape after the first flattening roll, but not too viscous, so that it could potentially stick to the roll.

4.1.2. Sigmacell cellulose

The Sigmacell cellulose solution was made with a cellulose content of 7 wt%, which was chosen in the previous chapter 4.1.1. **Figure 27** shows a representative viscosity curve against the shearing rate. The same tendency as with the cellulose solutions prepared with C6288 is observed. It has to be pointed out is that the viscosity of the Sigmacell cellulose solution (1.39 Pa·s) at a shear rate of 1000 1/s is significantly higher than the cellulose solution with the C6288 cellulose with the same weight percentage (0.39 Pa·s).

The increase of viscosity using the Sigmacell cellulose instead of the C6288 cellulose is probably due to a higher DP value in the Sigmacell cellulose. This leads to more entanglements and more interactions between the longer cellulose chains. Even though the Sigmacell cellulose solution has a viscosity about 3.5 times higher than the C6288 cellulose solution, it is still going to be considered as a reference for aerogel sheet production as it still seems to have an appropriate viscosity for the upscaling process.

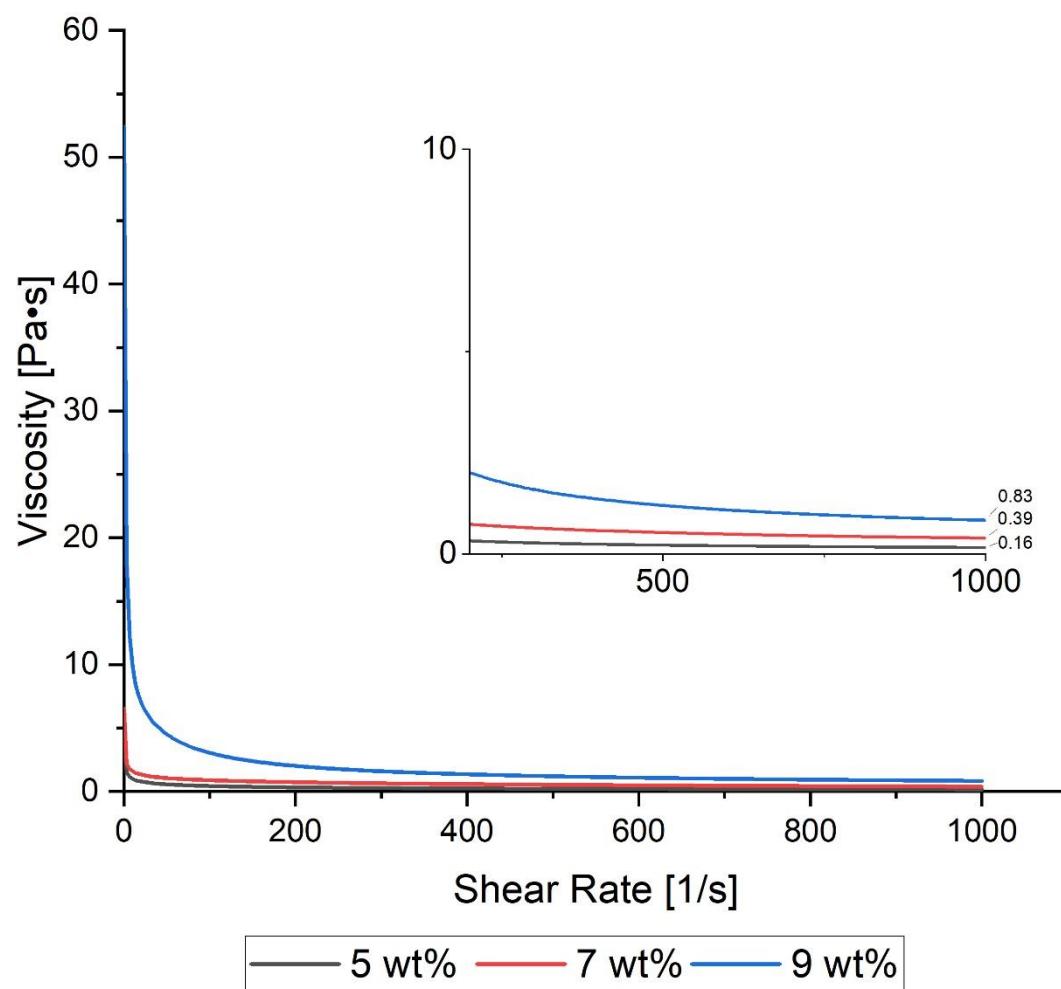


Figure 26: Cellulose solution viscosities with different weight concentration of C6288.

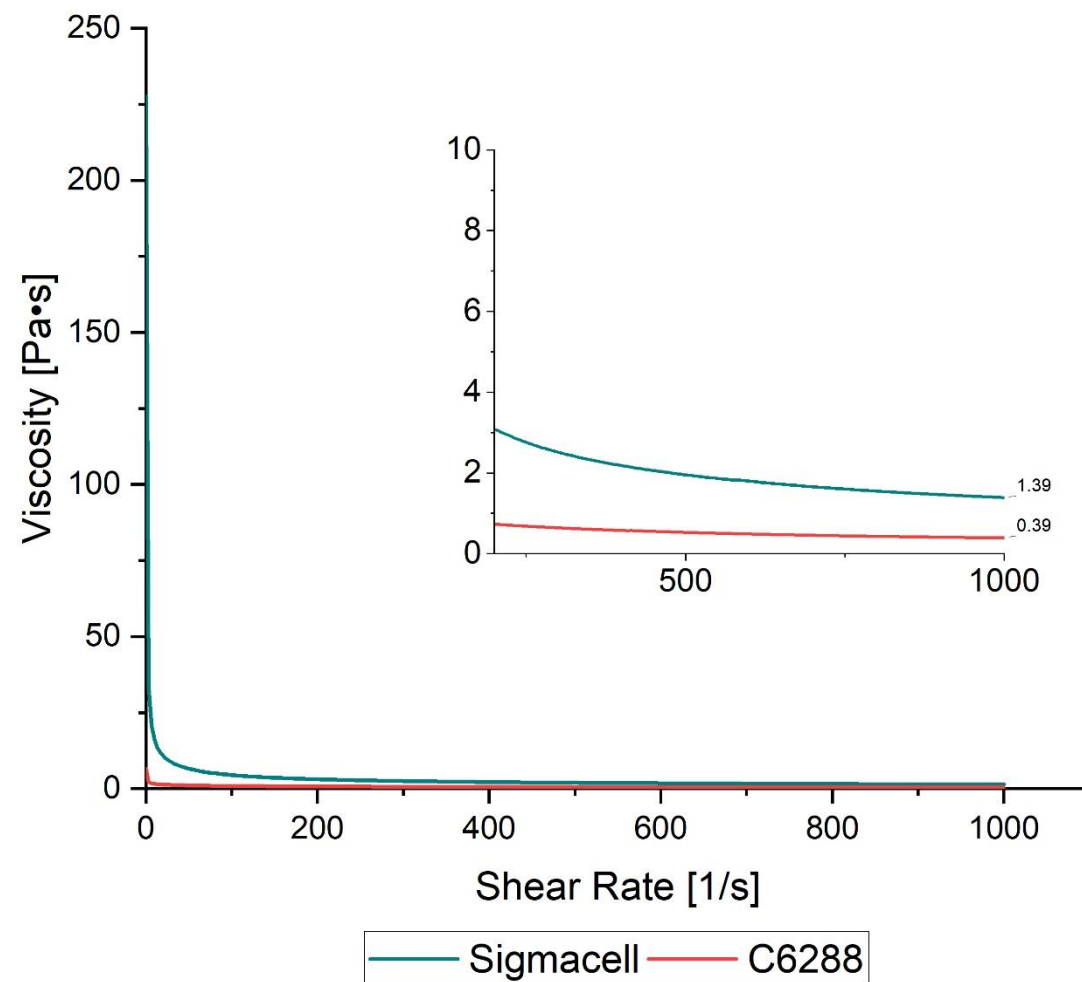


Figure 27: Comparison of Sigmacell and C6288 cellulose viscosity (7 wt%).

4.1.3. Hemp cellulose

Figure 28 shows a representative viscosity curve of cellulose solutions with an amount of 3 wt% and 5 wt% hemp cellulose. The known tendency of the previous chapters is observed. With increasing shear rate the viscosity is reduced, having a more pronounced effect analyzing the cellulose solution with higher hemp cellulose amount. The viscosity of the cellulose solution with 5 wt% of hemp cellulose (2.18 Pa·s) is about 3.5 times higher than the 3 wt% hemp cellulose solution (0.63 Pa·s).

To get a hemp solution with suitable properties to be used in the CaProLi device a viscosity between the 7 wt% cellulose solutions of C6288 and Sigmacell should be chosen. Therefore, the cellulose solution with 3 wt% of hemp cellulose is selected to proceed on the CaProLi device.

4.1.4. Comparison

Table 7 shows the concentrations, as well as the average viscosities (at shear rate of 1000/s) of the chosen solutions to proceed in this work. The Sigmacell cellulose solution has the highest viscosity followed by the hemp cellulose solution. The C6288 solution has the lowest viscosity of all cellulose solutions. Noticeable is that the hemp cellulose solution has reached a viscosity between both references cellulose solutions having not even half of their concentration. This means that the hemp cellulose has even a higher DP value than the Sigmacell cellulose.

Table 7: Viscosity comparison of CaProLi cellulose solutions.

Samples	Conc. [wt%]	Viscosity at shear rate 1000/s [Pa·s]
C6288	7	0.43 ± 0.03
Sigmacell	7	1.37 ± 0.03
Hemp	3	0.62 ± 0.03

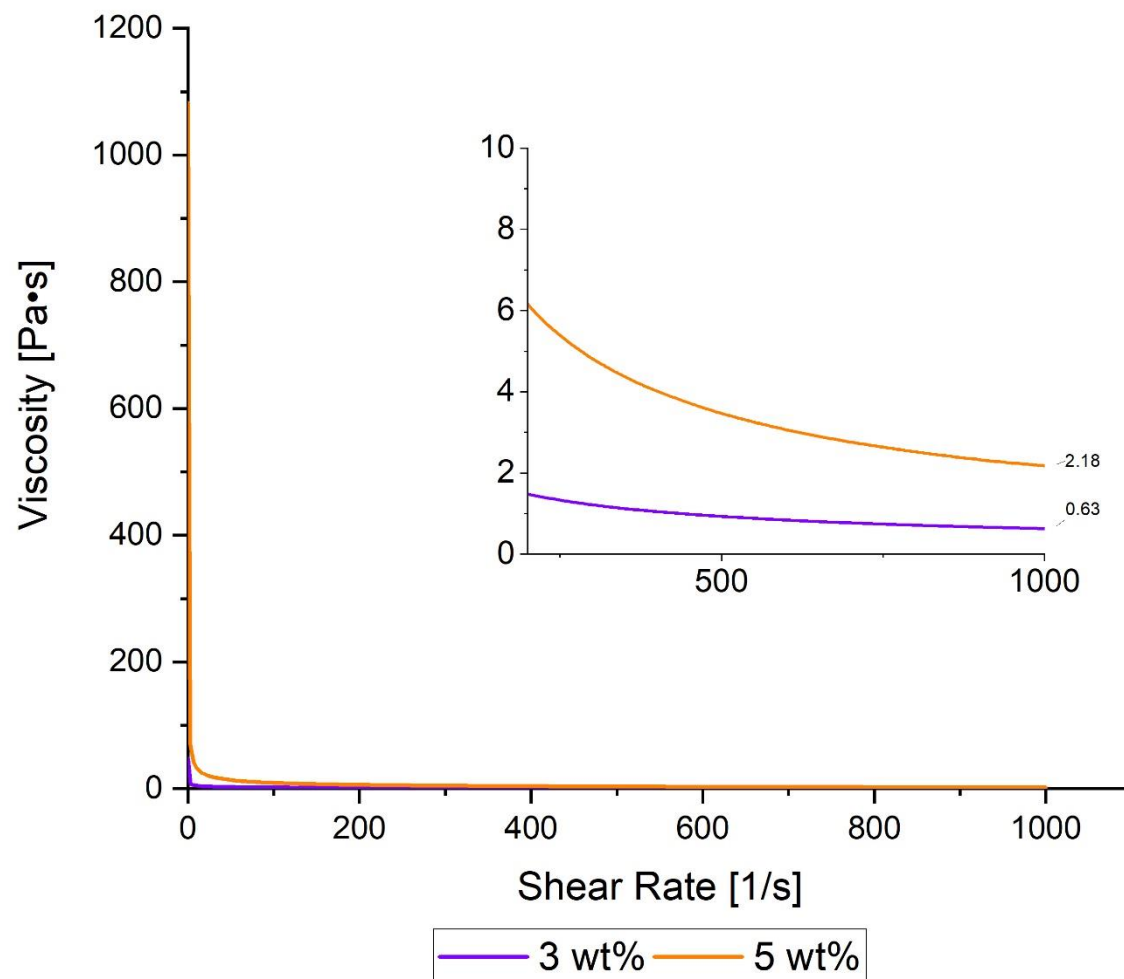


Figure 28: Viscosity of cellulose solutions with different concentrations of hemp cellulose.

4.2. Gel point

4.2.1. Cellulose solutions without salts

The gel points of the different cellulose solutions are shown in **Table 8**. It can be seen, that the C6288 cellulose reaches the gel point after 481.3 s (**Figure 29**), which means that the starting point of gelation is reached too slow for the usage in the CaProLi device. The Sigmacell cellulose solution has already passed the gel point in the beginning of the measurement (**Appendix I**). This is revealed by a higher G' than G'' in the beginning of the measurement. As a result, it can be possible to produce a solid sheet wet-gel body with the CaProLi device using the Sigmacell cellulose solution. The hemp cellulose solution achieves the gel point after 8.1 s (**Appendix II**), which means that it could be also possible using it on the CaProLi.

Looking on the data it can be deduced that higher cellulose solution viscosities lead to a faster gelation of them. This is probably derived to the cellulose chain length. A higher chain length results in more possible contact points to build a gel network. This would explain why the hemp cellulose solution reaches the gel point, nearly, right after the start of the measurement only having a 3 wt% cellulose amount (**Table 8**).

The Sigmacell cellulose solution is already a weak gel at the start of the analysis, therefore it can be tried out at on the CaProLi device without any additional improvement. The C6288 cellulose solution, as well is the hemp cellulose solution, will be tried to be improved. This will be done by adding sodium salt.

Table 8: Gel point comparison of cellulose solutions without salt.

Samples	Conc. [wt%]	Gel point [s]
C6288	7	481.3
Sigmacell	7	0.0
Hemp	3	8.1

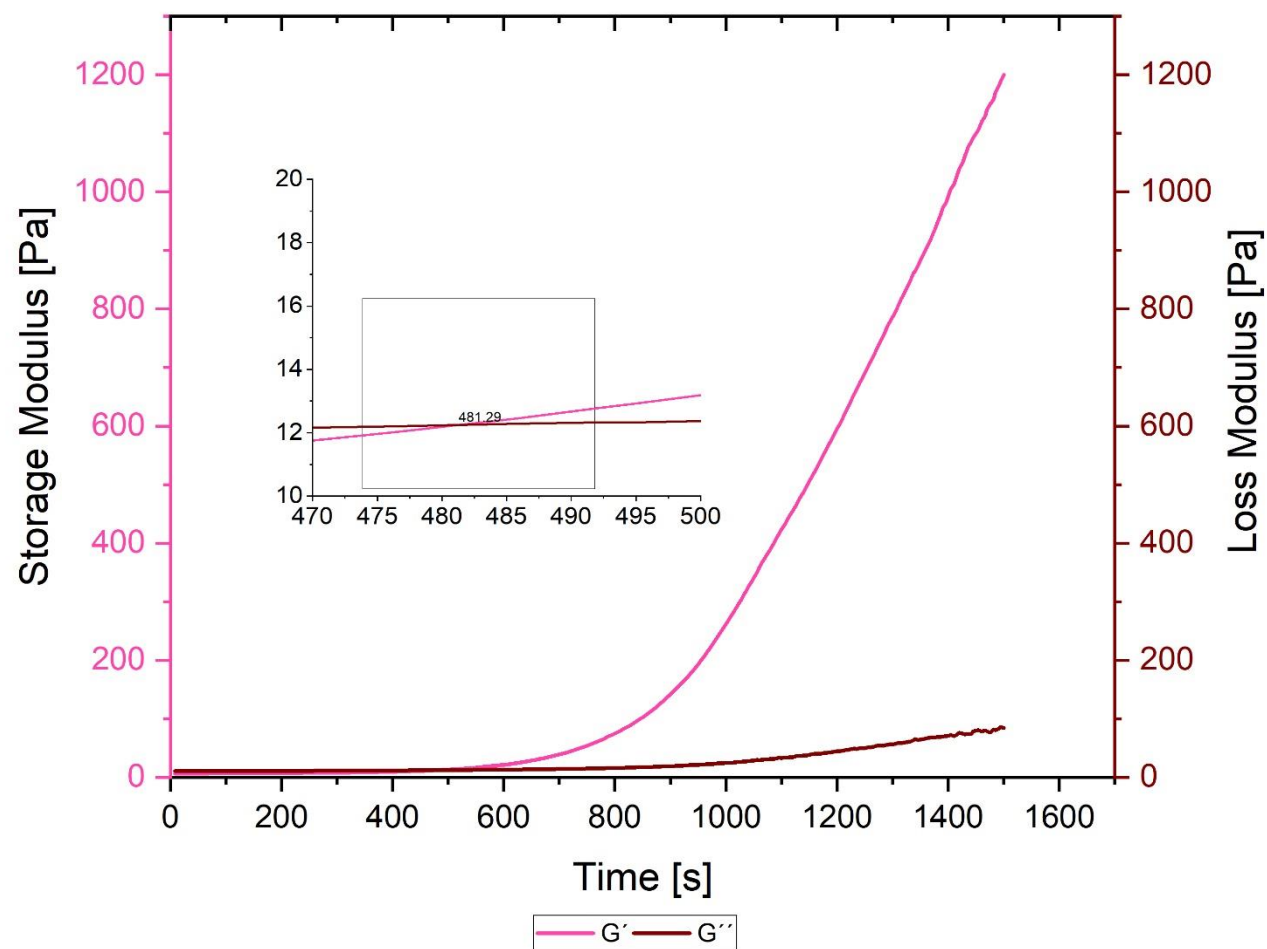


Figure 29: Example of gel point determination with C6288 cellulose solution.

4.2.2. Cellulose solutions with salts

To choose the better sodium salt and appropriate concentration of it, experiments were first made with addition to the C6288 cellulose solution. The results can be observed in **Figure 30-31**. It is shown that the addition of both sodium salts leads to a reduction of the gel point time, while having a stronger impact with increase of the salt concentration. The tendency seems to be linear for both salts. NaCl has a stronger effect on the reduction of the gel point time compared to Na₂SO₄. Therefore, NaCl is chosen as the salt to work with. To achieve a faster gelation, a concentration of 2 wt% NaCl is used in the C6288 cellulose solution (**Appendix III**) as well as in the hemp cellulose solution (**Appendix IV**).

The influence of salt addition on the reduction of the gel point time can be explained by the affinity of the salt ions to water. The ions compete with the cellulose chains for water and as they have a higher affinity they dehydrate the cellulose chains. This leads to a faster aggregation of the cellulose chains and therefore to a faster gelation [44, 65, 66]. One additional effect may also be a complex creation with urea and the anion of the corresponded salt.

4.2.3. Solutions for CaProLi experiment

Table 9 shows the solutions that are selected to proceed on the CaProLi device. With the addition of 2 wt% NaCl to the C6288 cellulose solution and to the hemp cellulose solution the gel point is reached before the measurement. Therefore, all cellulose solutions show good properties for the upscaling process. By comparing the G' of the different gels after 140 s it can be seen that the Sigmacell cellulose should have the strongest gel body and the C6288 cellulose the softest, close to hemp cellulose. A higher G' results in a stronger gel body [67].

Table 9: Gel point and storage modulus of the different cellulose CaProLi recipes.

Samples	Conc. [wt%]	NaCl conc. [wt%]	Gel point [s]	Storage modulus (140 s) [Pa]
C6288	7	2	0.0	47.2
Sigmacell	7	-	0.0	263.3
Hemp	3	2	0.0	56.6

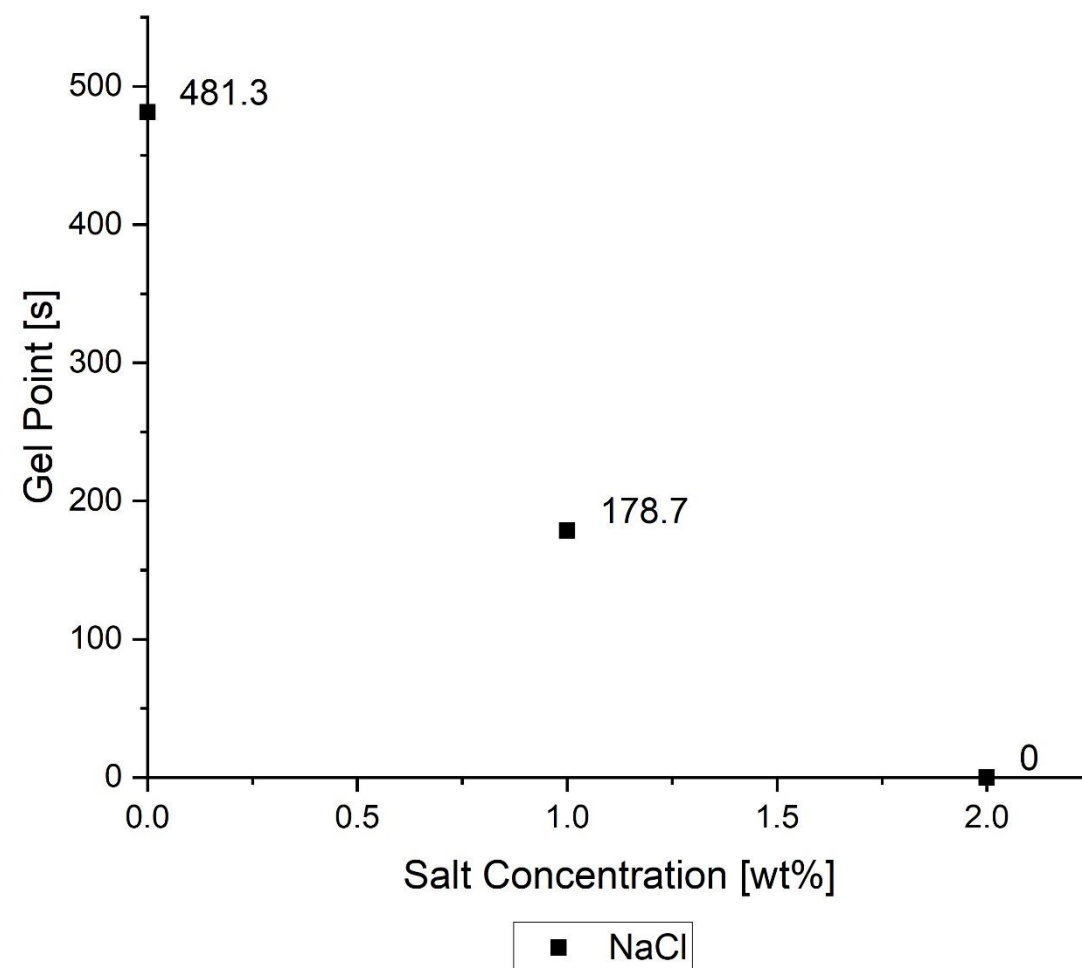


Figure 30: Tendency of gel point reduction with NaCl.

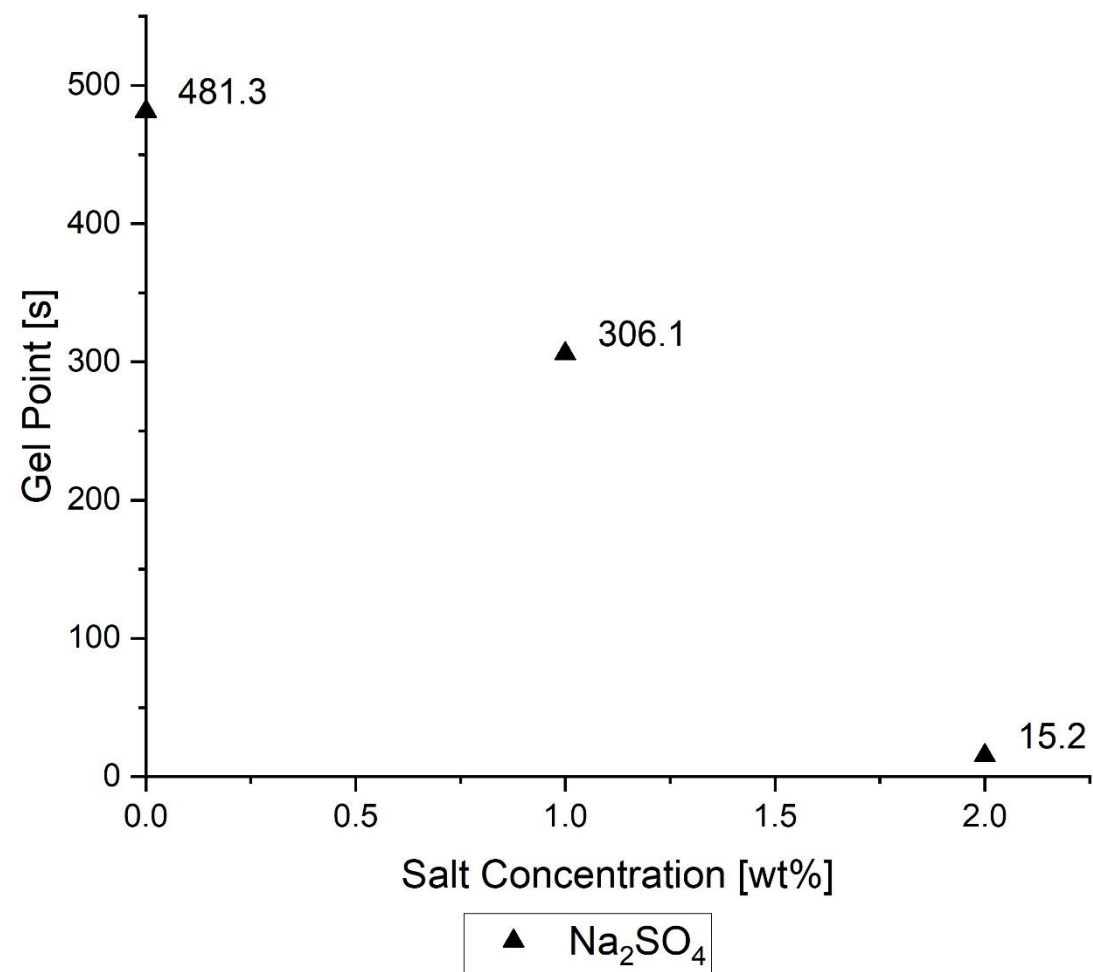


Figure 31: Tendency of gel point reduction with Na_2SO_4 .

4.3. Densities

From here onwards, the following abbreviations will be used for the different aerogel samples:

Table 10: Abbreviations for aerogel samples.

Sample	Conc. [wt%]	Abbreviation (Monolith)	Abbreviation (Sheet)
C6288	7	CM	-
C6288 + 1 wt% NaCl	7	CM1Cl	-
C6288 + 1 wt% Na ₂ SO ₄	7	CM1SO ₄	-
C6288 + 2 wt% NaCl	7	CM2CL	CS2CL
C6288 + 2 wt% Na ₂ SO ₄	7	CM2SO ₄	-
Sigmacell	7	SM	SS
Hemp	3	HM	-
Hemp +2 wt% NaCl	3	HM2Cl	HS2CL

4.3.1. Skeletal density

The measured skeletal density of a cellulose aerogel is shown in **Table 11**. The value corresponds to the range in literature [68, 69] and is therefore taken for further procedure.

Table 11: Skeletal density of cellulose.

Sample	Skeletal density [g/cm ³]
CM	1.521 ± 0.006

4.3.2. Envelope density

Besides the recipes that should be used on the upscaling process, some more monolithic aerogels are made using the C6288 cellulose as well as monolithic samples of hemp cellulose without 2 wt% of NaCl. The aim of that is to look on the influence of salt addition on the properties. Furthermore, the influence of the two different sodium salts used are investigated

Table 12 shows the envelope densities of the different monolithic cellulose aerogels. Comparing the envelope densities of the reference cellulose types used in this work, leads to the conclusion that the Sigmacell cellulose has a higher envelope density than the C6288 cellulose. The monolithic samples made from the hemp cellulose have the lowest density. The addition of the salts didn't have a significant influence on the envelope density.

The reason for the Sigmacell monoliths having a higher envelope density than the C6288 monoliths is probably a higher DP value in the Sigmacell cellulose. Longer cellulose chains lead to more contact points between the cellulose chains which could create more crystalline regions. Additionally, they have the tendency to entangle more, reducing free volume [70, 71]. The hemp monoliths have the lowest density, because they have the lowest cellulose concentration. The same has been observed for other cellulose aerogels before [72, 73].

Table 12: Envelope density of aerogel samples.

Sample	Envelope density
CM	0.168 ± 0.005
CM1Cl	0.168 ± 0.005
CM1SO ₄	0.156 ± 0.004
CM2CL	0.159 ± 0.005
CM2SO ₄	0.172 ± 0.003
SM	0.220 ± 0.001
HM	0.110 ± 0.004
HM2Cl	0.111 ± 0.003

4.4. Porosity

The porosity of the samples used in the previous chapter is shown in **Table 13**. The samples which have the highest envelope density have the lowest porosity, due to less free space. The porosity range of the monolithic samples is between 85.6%-92.7%, which corresponds to the values given in literature [1]. Higher porosity values will benefit the thermal insulation. Therefore, the aerogel sheets made of the hemp cellulose recipe should have better heat insulation properties than the sheets made of the reference cellulose solutions.

Table 13: Porosity of aerogel samples.

Sample	Porosity [%]
CM	89.0 ± 0.3
CM1Cl	89.0 ± 0.3
CM1SO ₄	89.7 ± 0.2
CM2CL	89.5 ± 0.3
CM2SO ₄	88.7 ± 0.2
SM	85.6 ± 0.0
HM	92.8 ± 0.2
HM2Cl	92.7 ± 0.2

4.5. Volume shrinkage

Concerning the shrinkage of the monolithic aerogels made with the different cellulose types a general tendency is observed (**Figure 31**), except for the HM2Cl sample (**Figure 31**). After the gelation bath and the washing with distilled water, obtaining the hydrogel, the highest shrinkage is observed (**Appendix V**). Except for the HM2Cl sample, the shrinkage does not show significant changes after the solvent exchange with ethanol, forming the alcogel. After the supercritical drying all aerogels indicate shrinkage in comparison to the alcogels (**Appendix V**). Furthermore, it is noticed that the SM sample had the lowest shrinkage from hydrogel to aerogel. Looking at the influence of the salts on the shrinkage, there is no significant effect (**Appendix V**). The shrinkages of the monolithic samples made with the recipes that are used on the CaProLi device are shown in **Table 14**. It must be considered that not all monolithic samples had a perfect cylindrical shape.

The reason for the hydrogel having the highest shrinkage in comparison to the cellulose solution in the container is that gelation occurs. Not having shrinkage in the solvent exchange step can be explained by the usage of a stepwise increase of the ethanol concentration (chapter 3.3.4.). Different surface tensions of water and ethanol would normally cause pore collapse when completely exchanging them at once, which leads to a shrinkage in the resulting alcogel. The usage of a concentration gradient counterbalances this effect. A slightly faster exchange of the water/ethanol ratio (chapter 3.3.4.) with the CM2CL samples, could have caused a significant increased shrinkage. Shrinkage after supercritical drying is explained by CO₂ being a non-solvent for cellulose, which could cause pore collapse, in combination with the applied pressure, used to reach supercritical conditions [74, 75].

Table 14: Shrinkage of aerogels samples (CaProLi recipe).

Sample	Shrinkage (Hydrogel) [%]	Shrinkage (Alcogel) [%]	Shrinkage (Aerogel) [%]
CM2Cl	36.7 ± 7.3	39.9 ± 4.5	48.8 ± 1.8
SM	53.2 ± 11.2	55.0 ± 10.3	61.3 ± 5.6
HM2Cl	26.1 ± 3.2	38.5 ± 1.7	56.7 ± 3.7

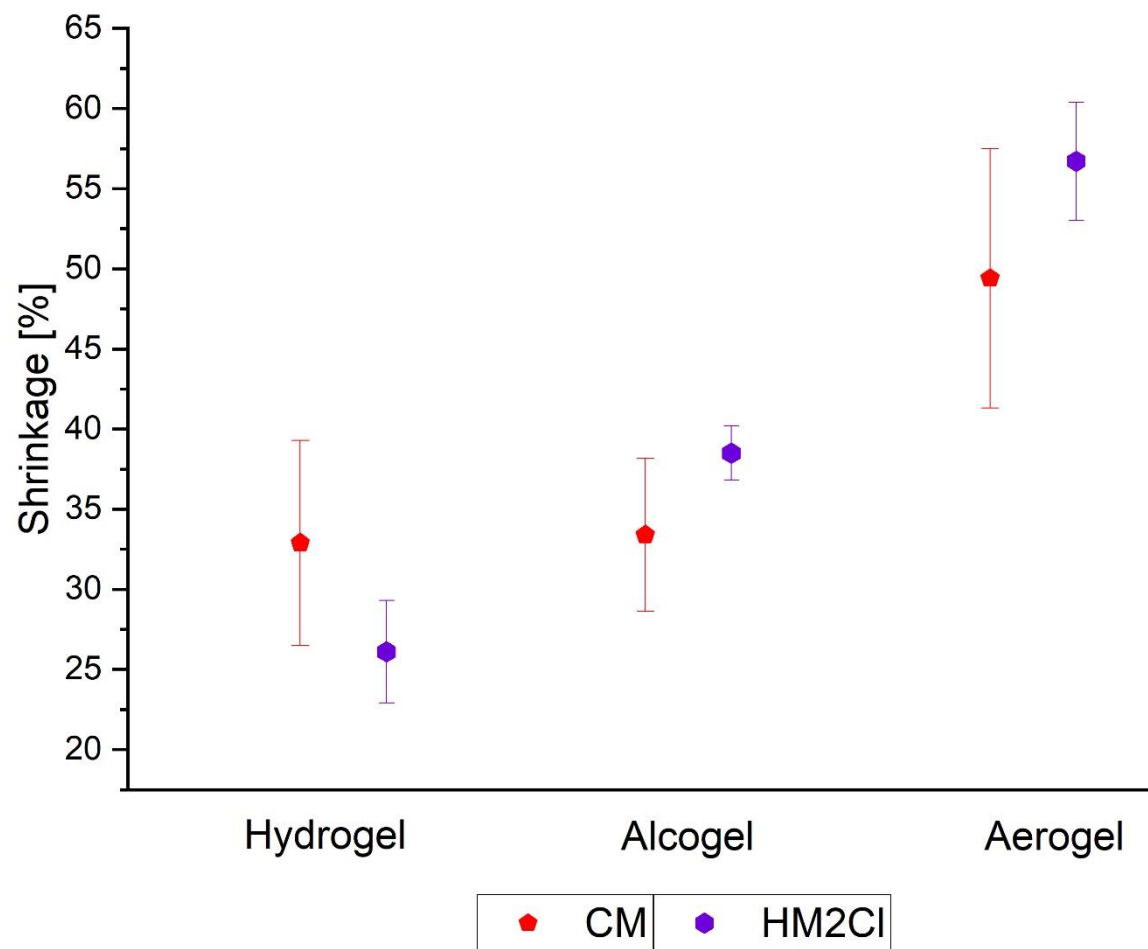


Figure 32: Tendency of volume shrinkage for almost all samples (ex. CM) and the HM2CI sample.

4.6. Gas sorption

4.6.1. Adsorption isotherm and BET surface

Figure 33 shows an example of a typical progression of the nitrogen adsorption-desorption isotherms for all measured aerogel samples. This is a characteristic isotherm for polysaccharide aerogels corresponding to a type IV shape. The well pronounced hysteresis at high relative pressures shows that the sample has mesopores [35].

Table 15 shows the specific BET surface area for the monolithic samples. The CM and SM sample show similar values around 260 g/cm^3 . In comparison, the HM sample has a surface area around 200 g/cm^3 . Looking at the influence of the NaCl and Na_2SO_4 , there is a slightly increase of the BET surface area with increasing amount of the salt content. NaCl shows a stronger effect, increasing the surface area of the CM sample around 20 % with the addition of 2 wt%. The same effect is observed in the HS2CL sample increasing the BET surface around 6 %.

The comparison of the monolithic samples with the sheet samples (**Table 16**), made on the CaProLi device, shows that there is a decrease of the BET surface considering the samples CS2Cl and SS. The HS2Cl sample shows a better surface area than the HM2Cl sample.

The reason for in increasement of the surface area with a higher salt content is that the salt particles cause more pores during the gelation, being between the cellulose chains. Additionally, the particles could make even more pores when being washed out of the gel body [44]. Changes in the BET surface area between the monolith and sheet samples can be explained by using a different gelation medium. On the CaProLi device a stronger acid was used in the gelation solution. Furthermore, the gelation solution had a higher acid content (20 wt%). Combining these two factors a faster gelation happened, probably resulting in a different morphology. Additionally, an inhomogeneity in the samples, could be the origin of different results between the sheet and monolith samples. This would also explain the different trends observed.

Table 15: BET surface area of monolithic aerogel samples.

Sample	BET surface [m²/g]
CM	258.5 ± 5.2
CM1Cl	283.9 ± 1.8
CM1SO ₄	270.6 ± 9.9
CM2CL	307.9 ± 12.7
CM2SO ₄	285.8 ± 2.6
SM	261.9 ± 8.3
HM	203.6 ± 6.7
HM2Cl	215.8 ± 4.6

Table 16: BET surface area of sheet shaped aerogel samples.

Sample	BET surface [m²/g]
CS2CL	287.7 ± 0.6
SS	193.8 ± 5.0
HS2Cl	264.4 ± 8.1

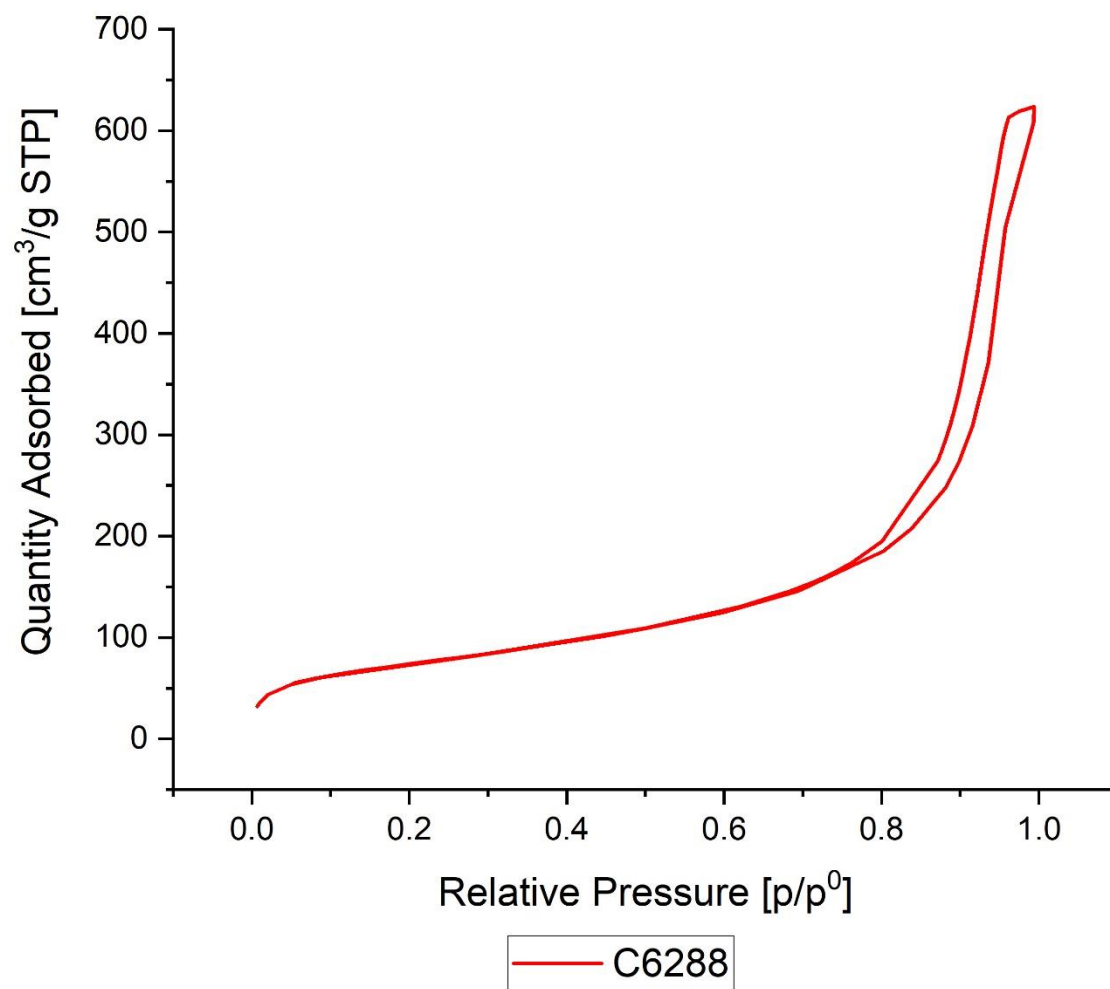


Figure 33: Exemplary adsorption isotherm of analyzed aerogel samples.

4.6.2. Pore distribution

The pore distributions of three different C6288 samples can be observed in **Figure 34** to look on the influence of salt addition, as well as comparing the monolithic and sheet samples. The pore distribution for the CM sample is approximately between 3-90 nm. Most of the pores are between 10-50 nm. This corresponds to a mesoporous material. The highest pore volume is about $1.75 \text{ cm}^3/\text{g}$. With the addition of 2 wt% NaCl a higher and larger peak with a little shift to the right side is observed showing an increment of pore volume with most pores being in bigger mesopores. This leads to an increase in pore quantity. Furthermore, higher pore widths in the macro pore area are observed, concluding a more porous material with increased pore distribution (~3-103nm). In comparison to the CM2Cl sample, the CS2CL sample shows an even higher peak with maximum pore volumes above $4.5 \text{ cm}^3/\text{g}$ between 30-40 nm. Additionally, the peak is a little thinner, showing an increase in mesopores with medium size and a decrease of macro pores.

Looking at the pore distributions of the Sigmacell samples the peak of SS sample is smaller, thinner and has a left shift compared to the SM peak showing a general decrease of pore amount and an emphasis in smaller mesopores (**Figure 35**). Main pore sizes are in both samples between 3-60 nm. What can be noticed is that the sheet sample has macro pores of a bigger size.

The pore distribution of the HM2Cl and the HS2Cl sample have a similar tendency compared to the Sigmacell cellulose samples, besides the small peak shift (**Figure 36**). The HM sample has a smaller quantity of mesopores compared to the HM2Cl and HS2Cl sample. Most of the pores are around 4-60 nm with sheet sample having bigger macro pores than the monolithic samples.

In general, it can be said that the addition of salt increases the amount of mesopores in the aerogel. The sheet has no significant difference compared to the same recipe in monolithic form. In the SS and HS2Cl sample bigger pores are observed compared to the monolithic samples. The CS2Cl and SS sample show a tighter pore distribution.

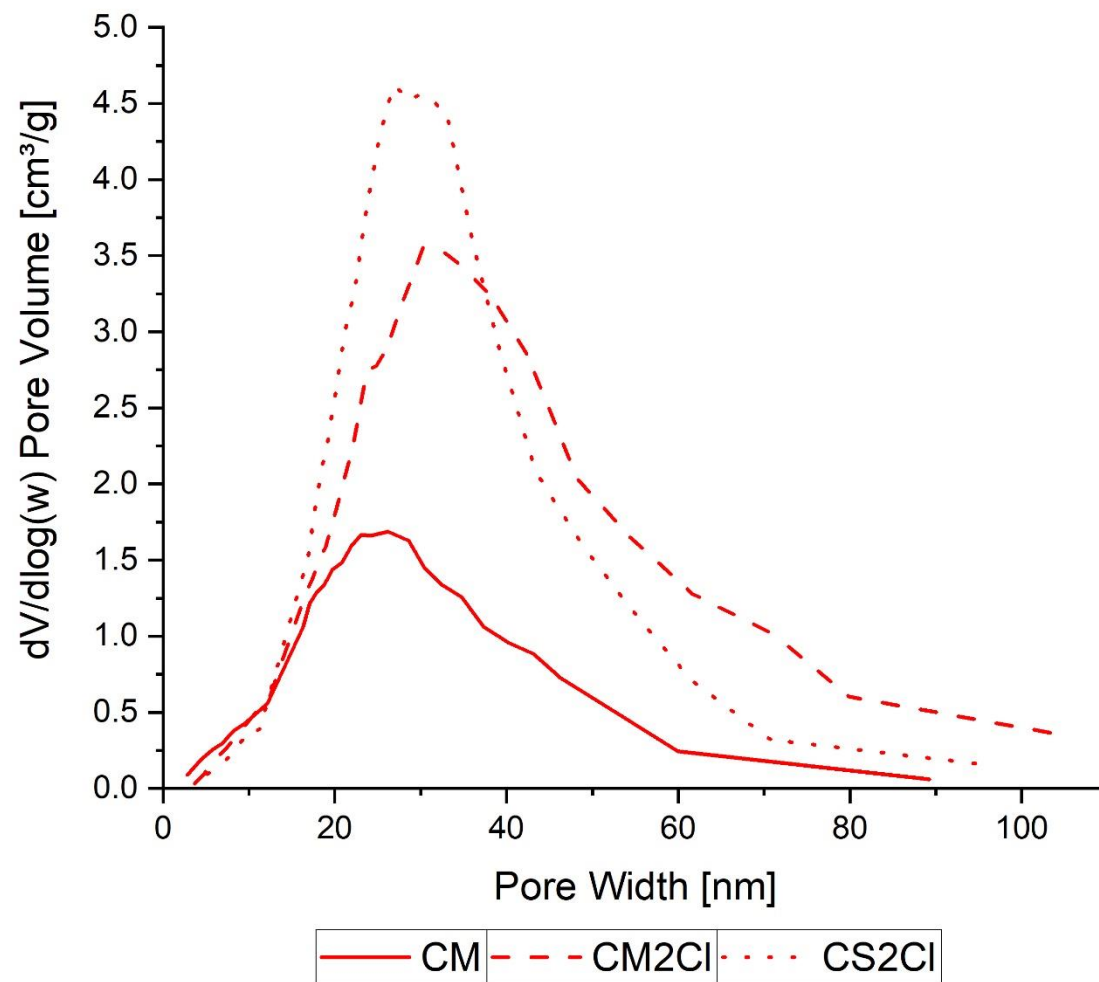


Figure 34: Pore size distribution C6288 samples.

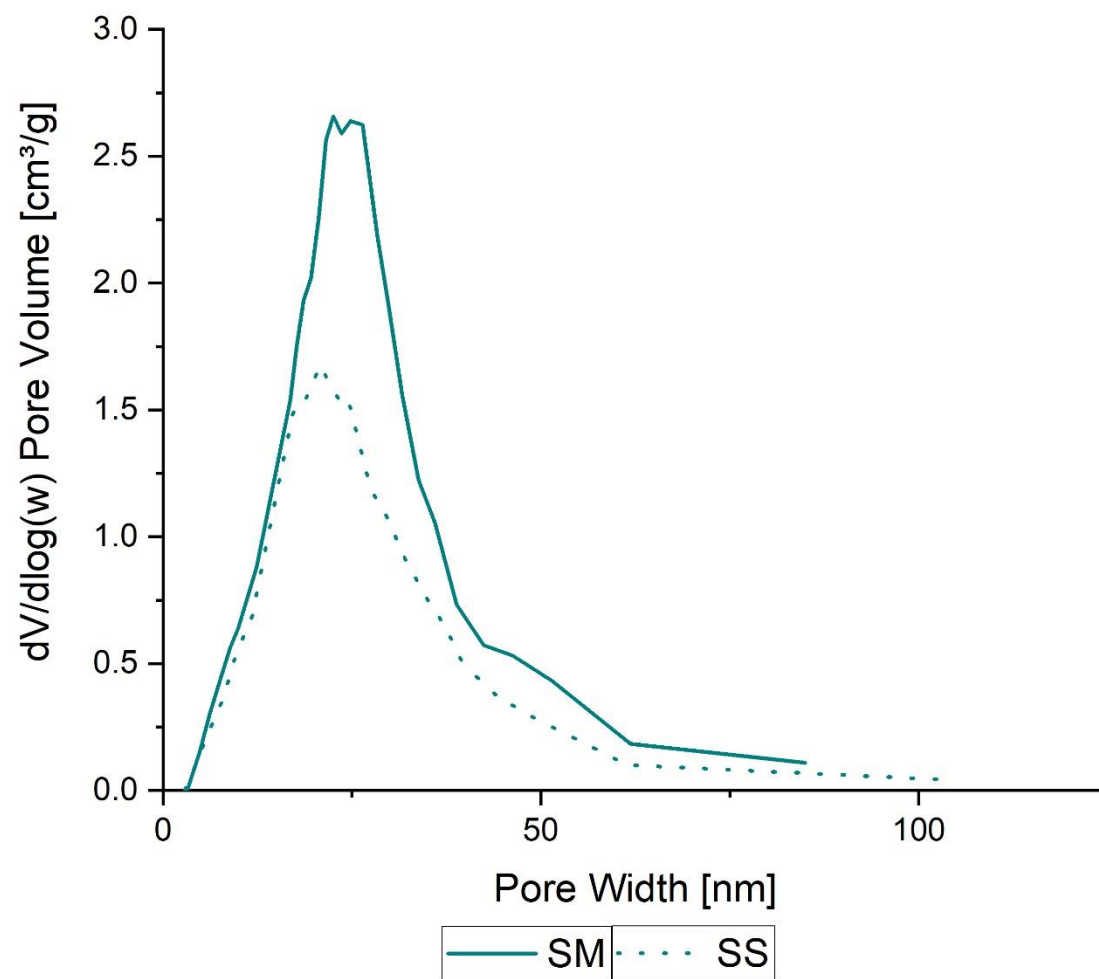


Figure 35: Pore size distribution Sigmacell samples.

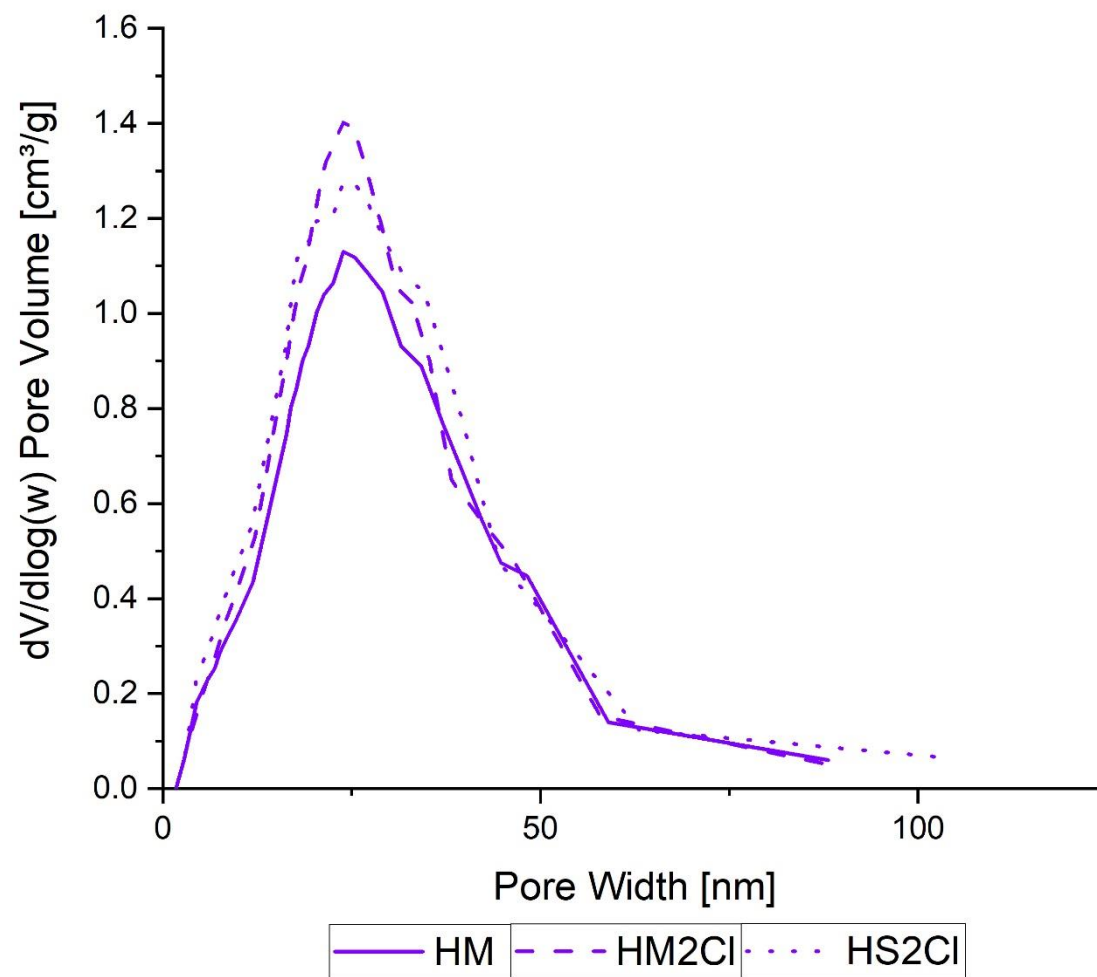


Figure 36: Pore size distribution hemp cellulose samples.

Table 17 and **Table 18** show values obtained from the BJH method. For the monolithic samples the average pore width is around 15 nm for every sample, which means that there is no significant change by adding NaCl. For the sheets the average pore width is higher for the samples made of C6288 cellulose. The Sigmacell cellulose sheets and the hemp cellulose sheets have no significant changes in comparison to the monoliths. Considering cumulative pore volume of the monolith samples, Sigmacell cellulose has the highest one, followed by the C6288 cellulose. The hemp cellulose has the smallest cumulative pore volume. The addition of NaCl increases the pore volume for the C6288 cellulose, but has no effect on the hemp cellulose. The sheets samples show an increase in the cumulative pore volume for the C6288 cellulose and a decrease for the Sigmacell cellulose. The hemp sheet does not show any significant changes. The difference in the values of both geometries may occur because of inhomogeneity.

Table 17: Average pore width and cumulative pore volume for monolithic aerogel samples.

Sample	Average pore width [nm]	Cumulative volume of pores [cm³/g]
CM	14.7 ± 0.7	0.99 ± 0.04
CM2CL	17.4 ± 3.8	1.40 ± 0.31
SM	15.2 ± 0.7	1.22 ± 0.02
HM	15.7 ± 3.0	0.85 ± 0.02
HM2CI	14.8 ± 1.0	0.83 ± 0.08

Table 18: Average pore width and cumulative pore volume for aerogel sheet samples.

Sheet Sample	Average pore width [nm]	Cumulative volume of pores [cm³/g]
CS2CL	21.5 ± 0.5	1.81 ± 0.06
SS	14.9 ± 0.5	0.95 ± 0.07
HS2CL	14.7 ± 1.5	1.01 ± 0.12

4.7. Morphology

Samples made with the CaProLi recipe for each cellulose are investigated with SEM. **Figure 37** shows the SEM pictures of a C6288 cellulose monolithic and sheet sample. Both samples show the typical randomly arranged 3D fibrillar network for cellulose aerogels [35, 76]. The monolithic sample has a much more pores in comparison to the sheet sample. The Sigmacell monolithic and sheet sample show the characteristic fibrillar 3D network (**Figure 38**) as well, but denser in comparison to the C6288 samples. Furthermore, the sheet sample seems to be a little bit denser when compared to the monolithic sample. The hemp samples show as well the fibrillar structure, but with a considerably longer fibril length compared to the samples of Sigmacell and C6288 cellulose, assuming a higher DP value. The porosity of the hemp samples is higher than the Sigmacell samples and seems to be comparable with the C6288 samples. The hemp sheet sample is more porous compared to the monolithic sample of hemp (**Figure 39**). In general, there is a difference between the morphology of the sheet and monolithic samples, which will be mainly due to the different gelation medium. Furthermore, it is shown that an addition of NaCl helps increasing the porosity of the 3D network (**Appendix VI**), probably due to the mentioned presence during gelation and washing.

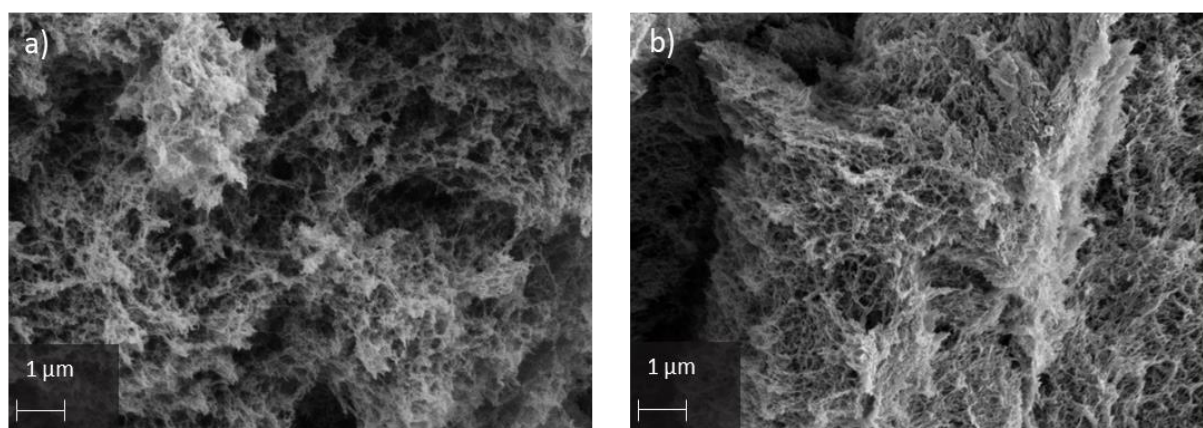


Figure 37: SEM images C6288: a) CM2Cl; b) CS2Cl.

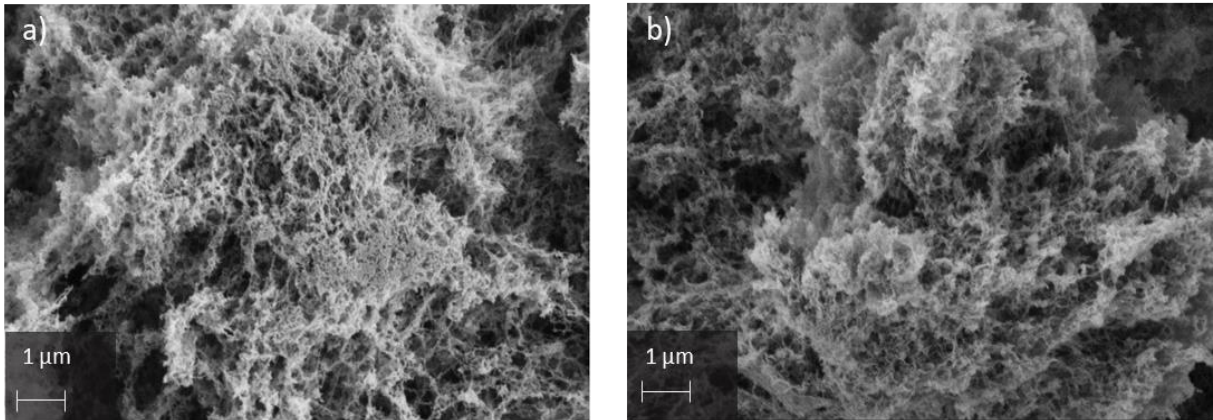


Figure 38: SEM images Sigmacell: a) SM; b) SS.

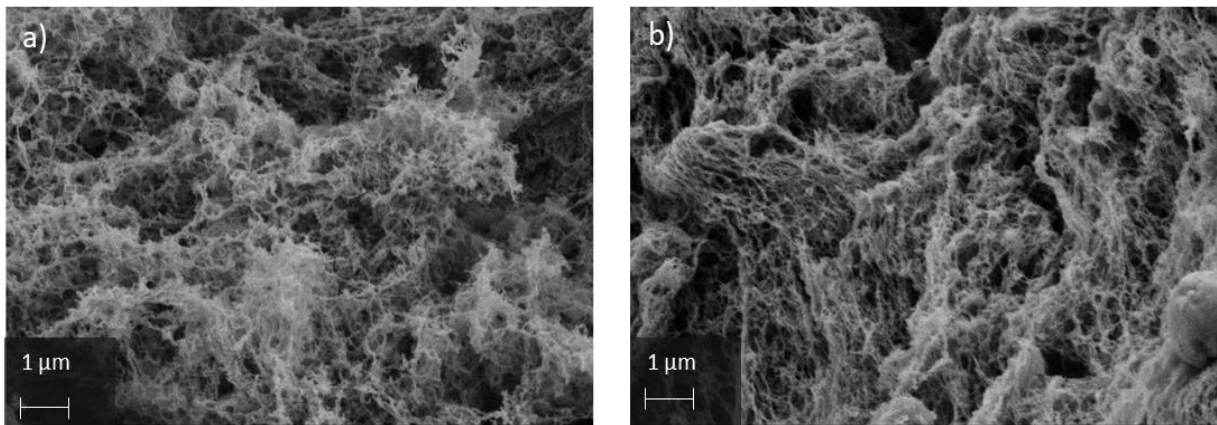


Figure 39: SEM images hemp cellulose: a) HM2Cl; b) HS2Cl.

4.8. FTIR

Figure 40 shows the infrared spectrum of the hemp fibers and the extracted hemp cellulose. Furthermore, the most characteristic vibrations considering the components of hemp fibers are shown [77]. The peak around 3400 cm^{-1} refers to the intra- and intermolecular stretching of OH in hemicellulose and cellulose. The peak around 2925 cm^{-1} shows the symmetric methyl and methylene stretching in hemicellulose and cellulose. Stretching vibrations of carbonyl in pectin and waxes lead to the small peak around 1730 cm^{-1} . Adsorbed water leads to a OH bending peak around 1650 cm^{-1} . The peaks in the area of $995\text{-}1202\text{ cm}^{-1}$ correspond to ring and side group vibrations of C-C, C-OH and C-H as well as to C-O-C stretching vibrations in cellulose and hemicellulose [77-79]. The difference between the infrared spectrum of the hemp fibers and the hemp cellulose is shown in **Figure 41**, when zooming in the area between $1200\text{-}2000\text{ cm}^{-1}$. The hemp fibers show a peak around 1246 cm^{-1} , which corresponds to the stretching of C=O and the guaiacyl ring in lignin [77]. This peak is not present in the hemp cellulose, meaning that lignin could be successfully removed. The peaks shown between $1500\text{-}1600\text{ cm}^{-1}$ in the hemp fibers strengthen this fact. The C=C stretching also corresponds to lignin [77]. These peaks are not present in the extracted hemp cellulose. It can be also seen that the pectin and the waxes were removed by the disappearing of the C=O stretching peak in the hemp cellulose. The comparison of the infrared spectra of hemp cellulose and C6288 cellulose shows that there is no difference in the obtained peaks, indicating a successful extraction of hemp cellulose (**Figure 42**).

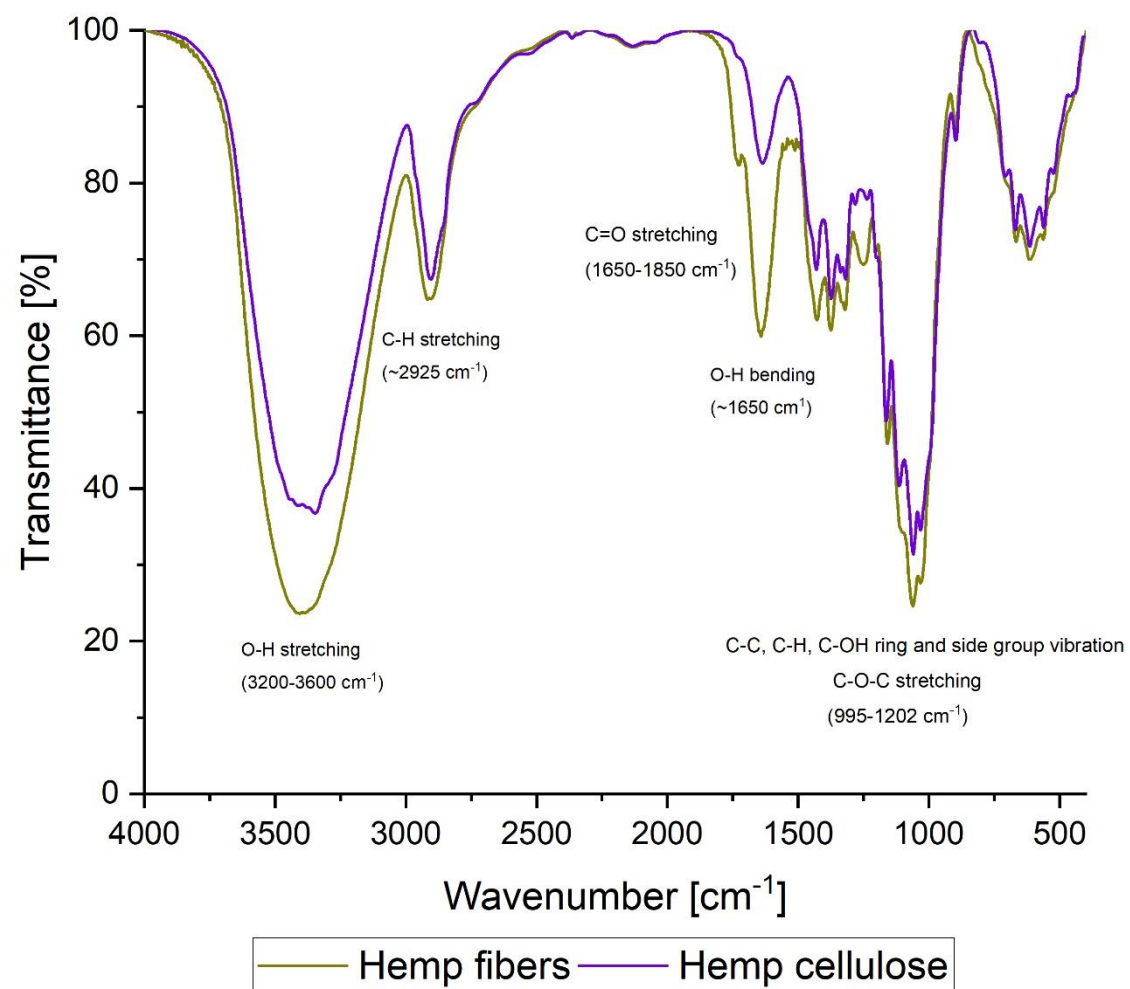


Figure 40: FTIR of milled hemp and hemp cellulose.

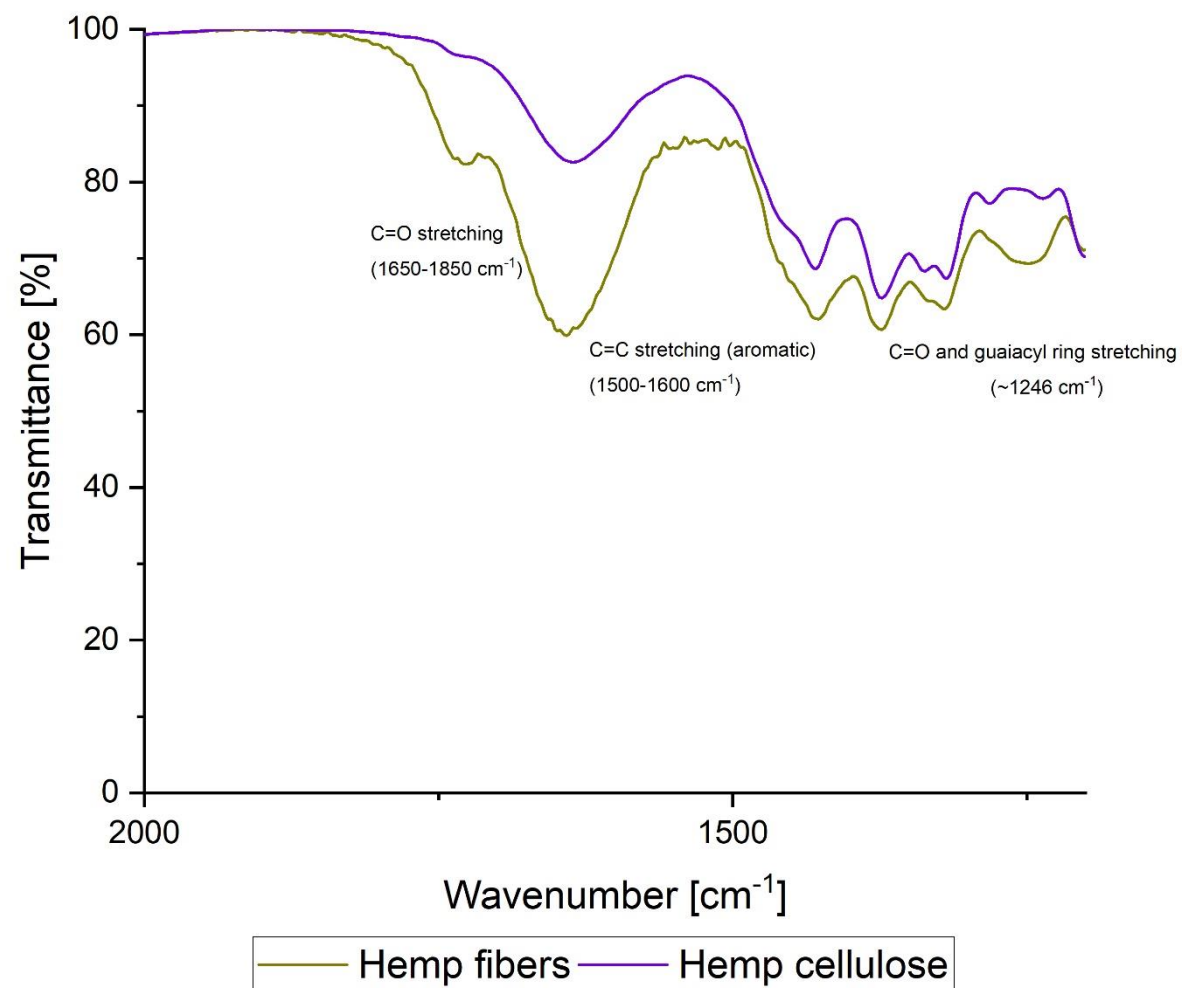


Figure 41: FTIR of milled hemp and hemp cellulose (zoom at area $1200\text{-}2000\text{ cm}^{-1}$).

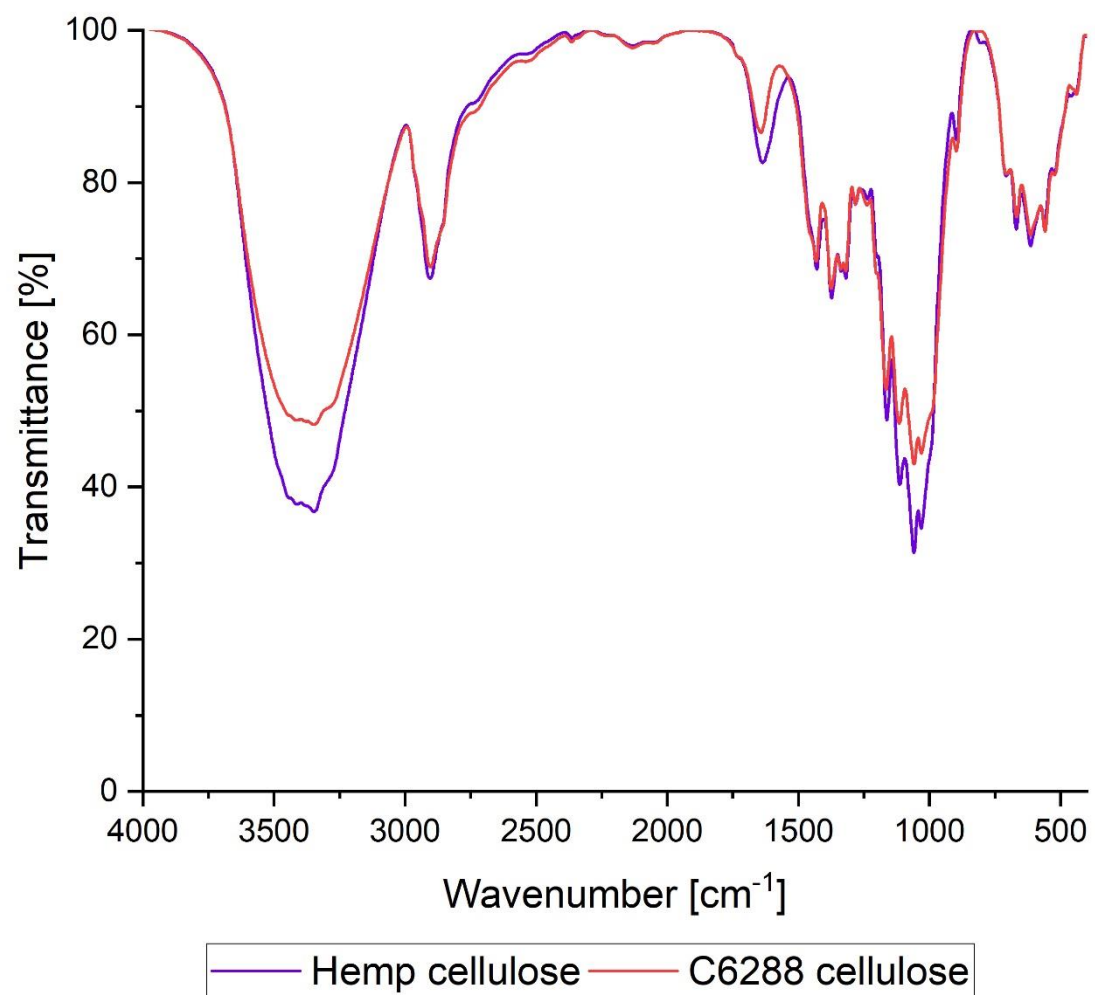


Figure 42: FTIR of hemp cellulose and C6288 cellulose.

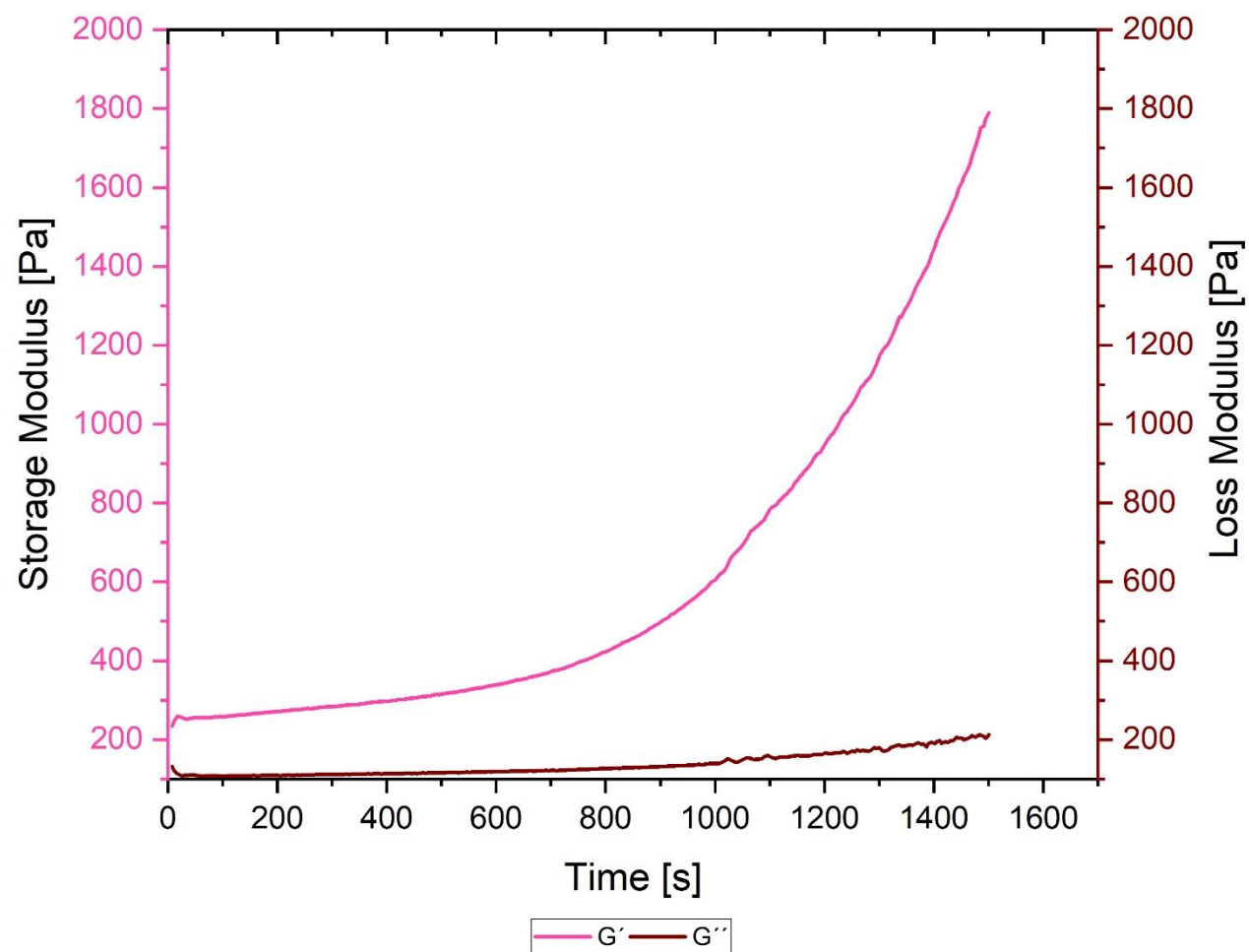
5. Conclusions

During this work aerogel sheets of hemp cellulose could be successfully made with an upscaling process using the CaProLi device. The aim of it was to use the sheets as cellulose insulation boards. Unexpected, the produced sheets have a thickness of < 0.3 mm and a therefore not suitable for the foreseen application, the usage as cellulose insulation board. Considering this, the recipe for the CaProLi device has still to be optimized to achieve a faster gelation of the gel body with a higher thickness. Additionally, this would also improve the strength of the gel, considering that the gel bodies obtained in this work were still a bit fragile. Improving that recipe and achieving stronger gel bodies could also be useful for a continuous production of hemp cellulose sheets on the CaProLi device. Worth mentioning is the usage of only 3 wt% of hemp cellulose for the upscaling recipe in comparison to the 7 wt% of cellulose in the reference solutions. This results in savings of resources, leading to cost reduction.

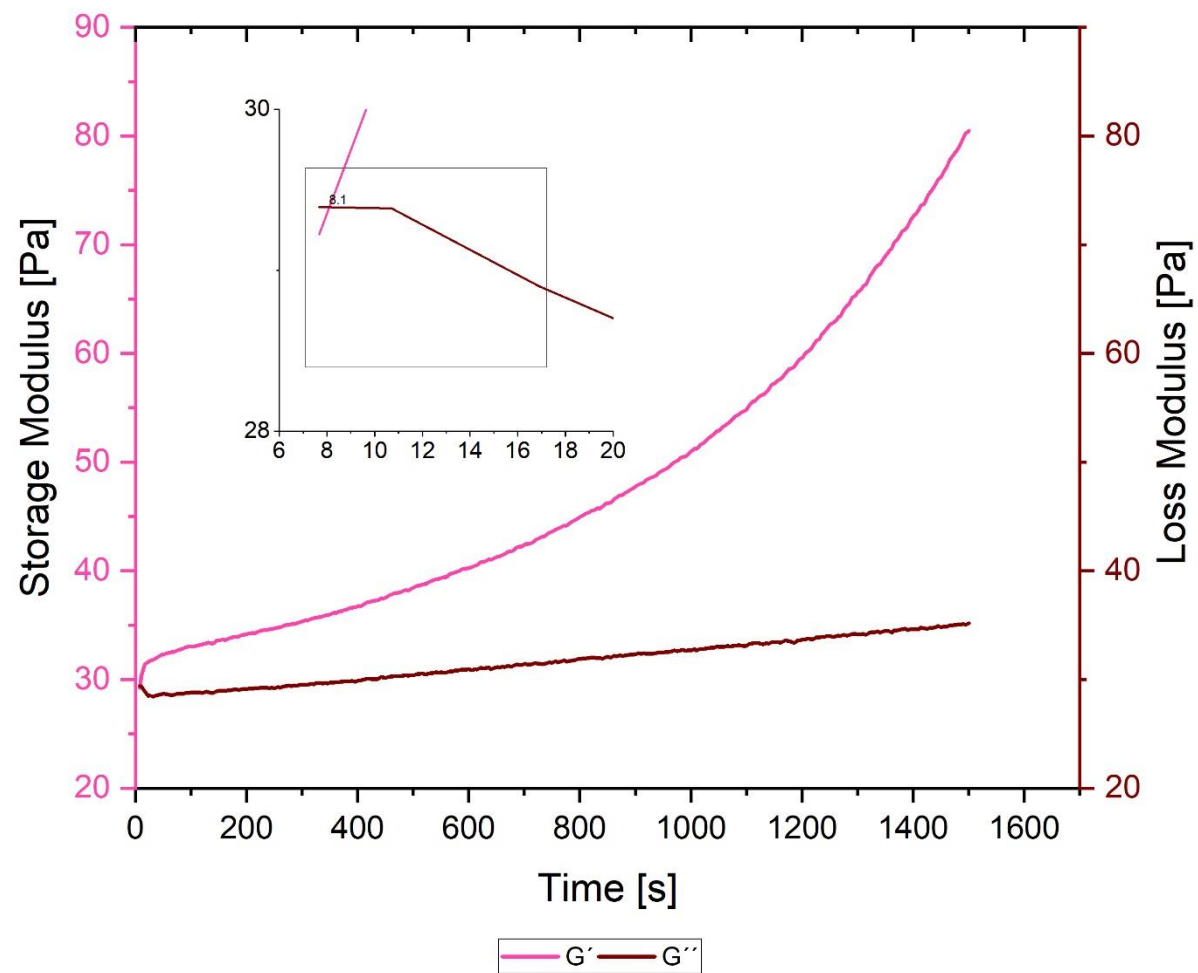
Moreover, the aerogel properties of the different cellulose types were investigated. The aim was to compare the cellulose types, the influence of salt addition and the different geometries made. It was shown that the hemp cellulose has the highest porosity (~93%), being, in this aspect, best suitable for heat insulation. The BET surface area of the hemp cellulose showed good values for the sheet samples, being near to the C6288 cellulose with the highest values also assuming good heat insulation properties. Total shrinkage was for all cellulose aerogels around 50% or more, which has to be considered in future dimension planning of the hemp cellulose boards. The addition of salt improved some properties, namely gelation time and BET surface area. The reduction of the gelation time made it possible to use a lower cellulose concentration in the C6288 cellulose and in the hemp cellulose, achieving stronger gel bodies in a shorter time. A positive side effect is the improvement of the BET surface area, which leads to better heat insulation. Changes of properties in the different geometries can also be detected, which is mainly attributed to the different gelation solution used.

To improve the recipe for the usage in the CaProLi a higher amount of hemp cellulose should be tried in combination with 2 wt% of NaCl. A concentration of 4 wt% hemp cellulose should be tried out to achieve thicker gel sheets. This will surely improve the strength as well as the gelation time to generate a thicker gel sheet. For operating with solutions, having higher concentrations of hemp cellulose, it is recommended to work with pressure and a slit die nozzle to pour the cellulose solution on the conveyor belt of the CaProLi. This will decrease the viscosity before going through the first flattening roll, considering that the viscosity was double as high compared to the Sigmacell solution.

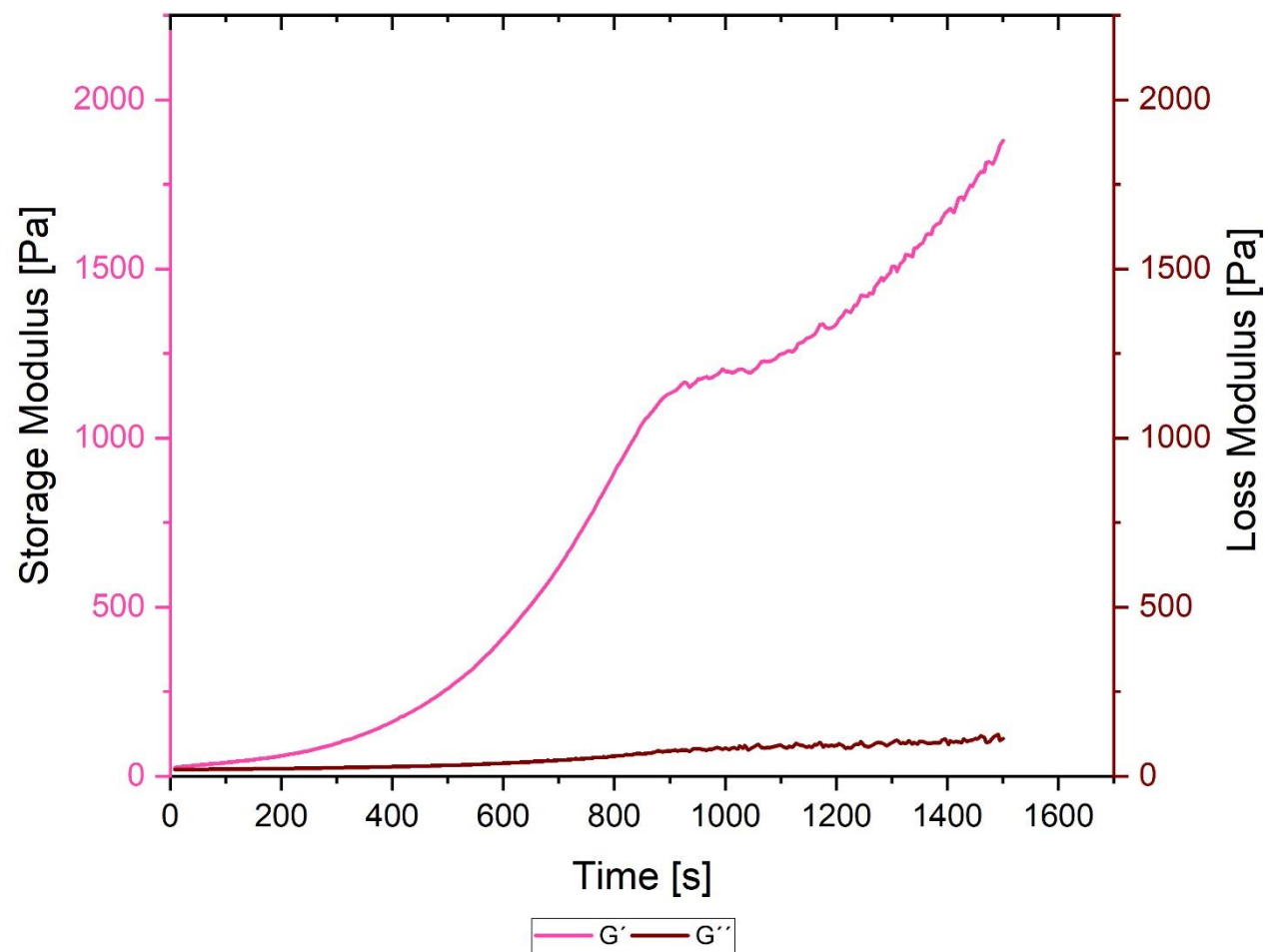
Appendix



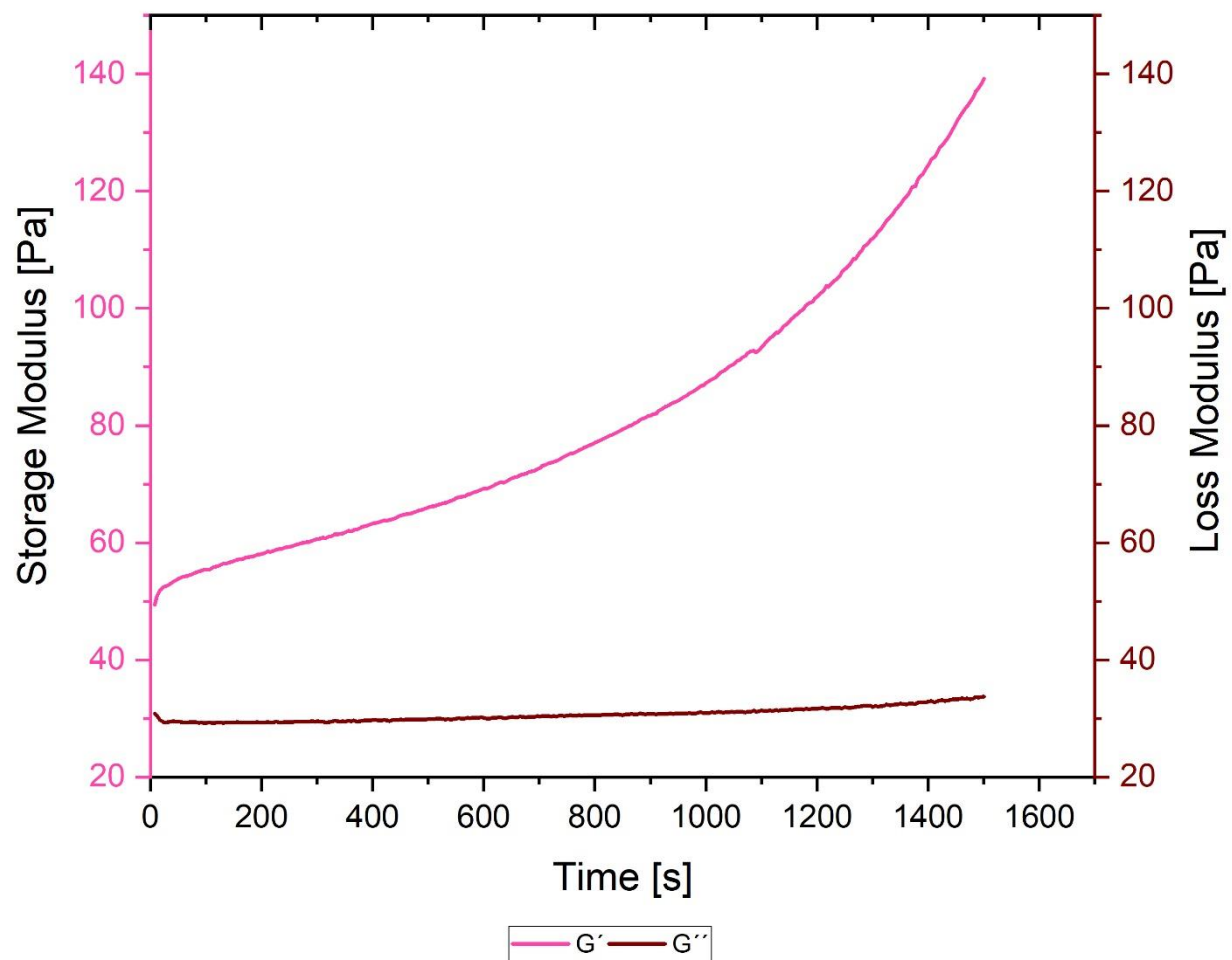
Appendix I: Gel point Sigmacell cellulose solution



Appendix II: Gel point hemp cellulose solution.



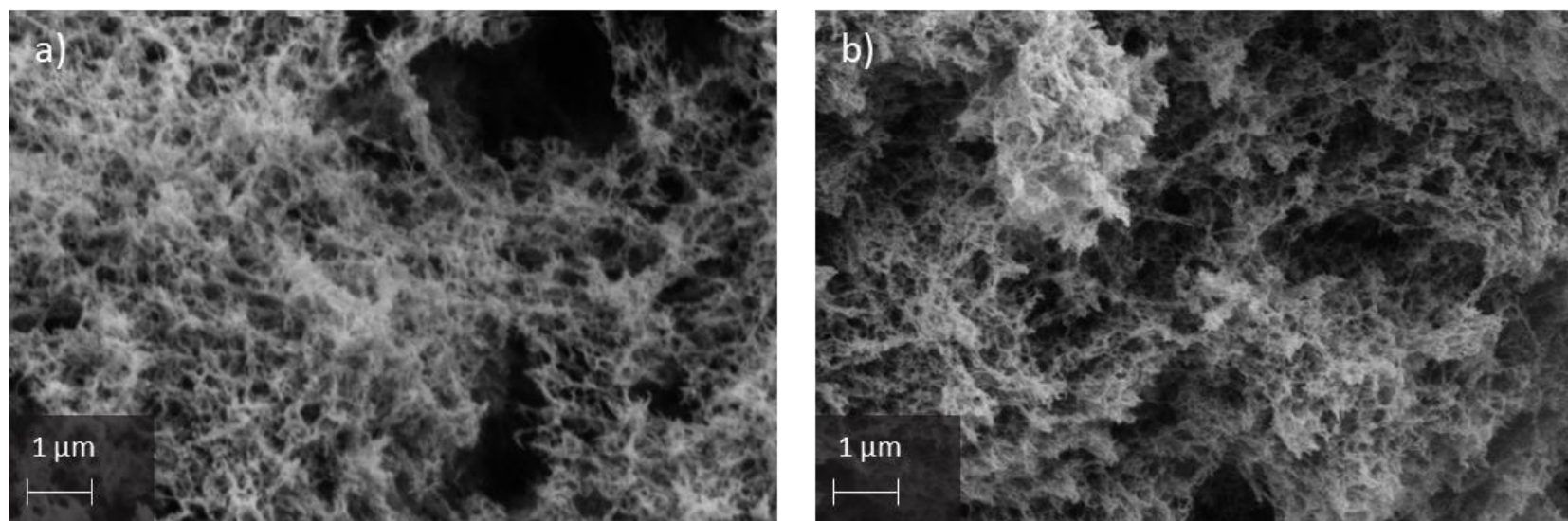
Appendix III: Gel point C6288 cellulose solution with 2 wt% NaCl.



Appendix IV: Gel point hemp cellulose solution with 2 wt% NaCl.

Appendix V: Shrinkages of monolithic samples.

Sample	Shrinkage (Hydrogel) [%]	Shrinkage (Alcogel) [%]	Shrinkage (Aerogel) [%]
CM	32.9 ± 6.4	33.4 ± 4.8	49.4 ± 8.1
CM1CL	44.7 ± 10.4	46.4 ± 10.7	56.8 ± 5.7
CM1SO4	40.9 ± 3.5	45.4 ± 7.1	53.7 ± 5.9
CM2Cl	36.7 ± 7.3	39.9 ± 4.5	48.8 ± 1.8
CM2SO4	36.3 ± 4.0	37.3 ± 3.4	50.9 ± 2.2
SM	53.2 ± 11.2	55.0 ± 10.3	61.3 ± 5.6
HM	30.5 ± 5.6	39.7 ± 6.2	57.2 ± 4.8
HM2Cl	26.1 ± 3.2	38.5 ± 1.7	56.7 ± 3.7



Appendix VI: Salt influence on morphology: a) CM; b) CM2Cl.

Literature

1. Long, L.Y., Y.X. Weng, and Y.Z. Wang, *Cellulose Aerogels: Synthesis, Applications, and Prospects*. Polymers (Basel), 2018. **10**(6).
2. Papavassiliou, D.V. and Q.T. Nguyen, *Flow and Heat or Mass Transfer in the Chemical Process Industry*. 2018: MDPI AG.
3. Pfundstein, M., et al., *Insulating Materials: Principles, Materials, Applications*. 2012: Birkhäuser.
4. Belwal, T. and N.C. Belwal, *Revolutionizing the Potential of Hemp and Its Products in Changing the Global Economy*. 2022: Springer International Publishing.
5. Basu, P., *Biomass gasification, pyrolysis and torrefaction: practical design and theory*. 2018: Academic press.
6. Nzihou, A., *Handbook on characterization of biomass, biowaste and related by-products*. 2020: Springer.
7. de Brito, J., et al., *Waste and Byproducts in Cement-Based Materials: Innovative Sustainable Materials for a Circular Economy*. 2021: Elsevier Science.
8. Northwest Advanced Bio-Fuels LLC. [cited 2021 22.12]; Available from: <https://nwabiofuels.com/woody-biomass-to-sustainable-aviation-fuels/>.
9. Living Wales. [cited 2021 22.12]; Available from: <https://wales.livingearth.online/data/environmental-variables/land/vegetation/herbaceous-biomass/>.
10. Beston. [cited 2021 22.12]; Available from: <https://bestonmachinery.com/de/charcoal-making-machine-in-cote-divoire/>.
11. Reset. [cited 2022 21.07]; Available from: <https://reset.org/biofuel-breakthrough-new-method-turns-algae-fuel-quicker-and-cheaper-ever-04092019/>.
12. NRDC. [cited 2022 21.07]; Available from: <https://www.nrdc.org/stories/composting-101>.
13. Adobe Stock. [cited 2022 21.07]; Available from: <https://stock.adobe.com/de/images/sheep-fur-wool-texture-closeup-background/188013510>.
14. Hussain, C.M., *Handbook of Polymer Nanocomposites for Industrial Applications*. 2020: Elsevier Science.
15. Bassam, N.E., *Handbook of Bioenergy Crops: A Complete Reference to Species, Development and Applications*. 2010: Taylor & Francis.
16. Hashim, N.O., *Hemp and the Global Economy: The Rise of Labor, Innovation, and Trade*. 2017: Lexington Books.
17. Dhondt, F. and S.S. Muthu, *Hemp and Sustainability*. 2021: Springer.
18. European Commission. [cited 2022 15.05.2022]; Available from: https://ec.europa.eu/info/food-farming-fisheries/plants-and-plant-products/plant-products/hemp_en.
19. Crellin, J.K., J. Philpott, and A.L.T. Bass, *Herbal Medicine Past and Present: A reference guide to medicinal plants*. 1990: Duke University Press.
20. Scholz, S.G., R.J. Howlett, and R. Setchi, *Sustainable Design and Manufacturing: Proceedings of the 8th International Conference on Sustainable Design and Manufacturing (KES-SDM 2021)*. 2021: Springer Singapore.
21. Foundation for Food & Agriculture Research. [cited 2022 21.07]; Available from: <https://foundationfar.org/consortia/hemp-research-consortium/>.
22. Duque, A., S. Pequito, and J. Pazour, *Industrial hemp fiber: A sustainable and economical alternative to cotton*. Journal of Cleaner Production, 2020. **268**: p. 122180.
23. Barbara, I., M. Daniela, and D. Tiziano, *Co-Corporeality of Humans, Machines, & Microbes*. 2022: Birkhäuser.
24. Rojas, O.J., *Cellulose chemistry and properties: fibers, nanocelluloses and advanced materials*. Vol. 271. 2016: Springer.

25. Thakur, V.K., M.K. Thakur, and M.R. Kessler, *Handbook of Composites from Renewable Materials, Structure and Chemistry*. 2017: Wiley.
26. Dominiak, K., *¹³C-NMR-spektroskopische Untersuchungen zur Substituentenverteilung in Cellulosexanthogenaten*. 2010.
27. Inamuddin, T.A.R., *Aerogels I: Preparation, Properties and Applications*. 2020: Materials Research Forum LLC.
28. Da Ros, T., N. Martín, and J.F. Nierengarten, *Carbon Nanostructures for Biomedical Applications*. 2021: Royal Society of Chemistry.
29. Popa, V.I., *Sustainability of Biomass through Bio-based Chemistry*. 2021: CRC Press.
30. Muthuraj, R., et al., *Applications of Polysaccharide and Protein Based Aerogels in Thermal Insulation*. 2018. p. 261-294.
31. Medronho, B., et al., *Rationalizing cellulose (in) solubility: reviewing basic physicochemical aspects and role of hydrophobic interactions*. *Cellulose*, 2012. **19**(3): p. 581-587.
32. Peters, J., *Strukturuntersuchungen an Cellulose und Cellulosederivaten aus ionischen Lösemitteln*. 2004.
33. Papageorgiou, G.Z., *Polymers from Renewable Resources*. 2019: MDPI AG.
34. Fricke, J. and A. Emmerling, *Aerogels*. *Journal of the American Ceramic Society*, 1992. **75**(8): p. 2027-2035.
35. Aegerter, M.A., N. Leventis, and M.M. Koebel, *Aerogels Handbook*. 2011: Springer New York.
36. Kuchta, L. and V. Fajnor, *About the synthesis and thermal stability of SiO₂-aerogel*. *Journal of thermal analysis*, 1996. **46**(2): p. 515-520.
37. Lichtfouse, E., S.S. Muthu, and A. Khadir, *Inorganic-Organic Composites for Water and Wastewater Treatment: Volume 2*. 2021: Springer.
38. Thomas, S., L.A. Pothan, and R. Mavelil-Sam, *Biobased Aerogels: Polysaccharide and Protein-based Materials*. 2018: Royal Society of Chemistry.
39. Ganesan, K., et al., *Review on the Production of Polysaccharide Aerogel Particles*. *Materials (Basel)*, 2018. **11**(11).
40. Acharya, S., et al., *Utilization of Cellulose to Its Full Potential: A Review on Cellulose Dissolution, Regeneration, and Applications*. *Polymers (Basel)*, 2021. **13**(24).
41. Budtova, T. and P. Navard, *Cellulose in NaOH-water based solvents: a review*. *Cellulose*, 2016. **23**(1): p. 5-55.
42. Xiong, B., et al., *Dissolution of cellulose in aqueous NaOH/urea solution: role of urea*. *Cellulose*, 2014. **21**(3): p. 1183-1192.
43. Cai, J. and L. Zhang, *Rapid Dissolution of Cellulose in LiOH/Urea and NaOH/Urea Aqueous Solutions*. *Macromolecular Bioscience*, 2005. **5**(6): p. 539-548.
44. Parajuli, P., et al., *Cellulose-based monoliths with enhanced surface area and porosity*. *Journal of Applied Polymer Science*, 2020. **137**(34): p. 48975.
45. Parajuli, P., et al., *Tuning the morphological properties of cellulose aerogels: an investigation of salt-mediated preparation*. *Cellulose*, 2021. **28**(12): p. 7559-7577.
46. Bertsch, P., S. Isabetтини, and P. Fischer, *Ion-Induced Hydrogel Formation and Nematic Ordering of Nanocrystalline Cellulose Suspensions*. *Biomacromolecules*, 2017. **18**(12): p. 4060-4066.
47. Figura, L. and A.A. Teixeira, *Food Physics: Physical Properties - Measurement and Applications*. 2007: Springer Berlin Heidelberg.
48. Bröckel, U., W. Meier, and G. Wagner, *Product Design and Engineering: Formulation of Gels and Pastes*. 2013: Wiley.
49. Bonten, C., *Kunststofftechnik: Einführung und Grundlagen*. 2020: Carl Hanser Verlag GmbH & Company KG.
50. Fernandez-Nieves, A. and A.M. Puertas, *Fluids, Colloids and Soft Materials: An Introduction to Soft Matter Physics*. 2016: Wiley.
51. Tanzi, M.C. and S. Fare, *Characterization of Polymeric Biomaterials*. 2017: Elsevier Science.
52. Koch, F.J., *X-ray optics made by X-ray lithography: Process optimization and quality control*. 2017: KIT Scientific Publishing.

53. Jewiarz, M., *Selected paper from 6th International Conference on Renewable Energy Sources (ICoRES 2019)*. 2020: MDPI AG.
54. Neikov, O.D., S. Naboychenko, and N.V. Yefimov, *Handbook of Non-Ferrous Metal Powders: Technologies and Applications*. 2018: Elsevier Science.
55. Litster, J., *Design and Processing of Particulate Products*. 2016: Cambridge University Press.
56. Flick, E.W., *Handbook of Adhesive Raw Materials*. 1989: Elsevier Science.
57. Tsotsas, E. and A.S. Mujumdar, *Modern Drying Technology, Volume 2: Experimental Techniques*. 2011: Wiley.
58. Yang, R.T., *Adsorbents: Fundamentals and Applications*. 2003: Wiley.
59. Preedy, V.R., *Selenium: Chemistry, Analysis, Function and Effects*. 2015: Royal Society of Chemistry.
60. Hertel, I.V. and C.P. Schulz, *Atoms, Molecules and Optical Physics 2: Molecules and Photons - Spectroscopy and Collisions*. 2014: Springer Berlin Heidelberg.
61. Pavia, D.L., et al., *Introduction to Spectroscopy*. 2014: Cengage Learning.
62. Sitotaw, Y.W., et al., *Ball milling as an important pretreatment technique in lignocellulose biorefineries: a review*. Biomass Conversion and Biorefinery, 2021.
63. Owonubi, S.J., et al., *Non-woody Biomass as Sources of Nanocellulose Particles: A Review of Extraction Procedures*. Frontiers in Energy Research, 2021. **9**.
64. Rodriguez, F., et al., *Principles of Polymer Systems*. 2014: CRC Press.
65. Park, H., et al. *Effect of Calcium Phosphate Precursor Salt on Gelation Temperature of Methylcellulose*. 2016.
66. Kundu, P.P. and M. Kundu, *Effect of salts and surfactant and their doses on the gelation of extremely dilute solutions of methyl cellulose*. Polymer, 2001. **42**: p. 2015-2020.
67. Zoveidavianpoor, M., *Current Topics in the Utilization of Clay in Industrial and Medical Applications*. 2018: IntechOpen.
68. Pircher, N., et al., *Impact of selected solvent systems on the pore and solid structure of cellulose aerogels*. Cellulose, 2016. **23**(3): p. 1949-1966.
69. Ganesan, K., et al., *Design of aerogels, cryogels and xerogels of cellulose with hierarchical porous structures*. Materials & design, 2016. **92**: p. 345-355.
70. Fetters, L.J., et al., *Connection between Polymer Molecular Weight, Density, Chain Dimensions, and Melt Viscoelastic Properties*. Macromolecules, 1994. **27**(17): p. 4639-4647.
71. Maier, C. and T. Calafut, *Polypropylene: The Definitive User's Guide and Databook*. 1998: Elsevier Science.
72. Hoepfner, S., L. Ratke, and B. Milow, *Synthesis and characterisation of nanofibrillar cellulose aerogels*. Cellulose, 2008. **15**(1): p. 121-129.
73. Arcari, M., et al., *Structure–property relationships of cellulose nanofibril hydro- and aerogels and their building blocks*. Nanoscale, 2020. **12**(21): p. 11638-11646.
74. Budtova, T., *Cellulose II aerogels: a review*. Cellulose, 2019. **26**(1): p. 81-121.
75. Lebedev, A., et al., *Investigation of aerogel production processes: Solvent exchange under high pressure combined with supercritical drying in one apparatus*. Gels, 2021. **7**(1): p. 4.
76. Karadagli, I., et al., *Synthesis and characterization of highly porous cellulose aerogels for textiles applications*. Proceedings Cellular Materials, Cellmat 2012, 2012.
77. Dai, D. and M. Fan, *Characteristic and Performance of Elementary Hemp Fibre*. Materials Sciences and Applications, 2010. **01**: p. 336-342.
78. Derrick, M.R., D. Stulik, and J.M. Landry, *Infrared Spectroscopy in Conservation Science*. 2000: Getty Conservation Institute.
79. Rives, V., *Layered Double Hydroxides: Present and Future*. 2001: Nova Science Publishers.